X-Ray Diffraction Study of Phase Transitions in TiO_2 and HfO_2 at High Pressure and High Temperature

Jie Tang

February 1993

Abstract

The phase transitions in the dioxides of the two elements, belonging to the same IVa group, Ti and Hf, were studied by *in situ* X-ray diffraction under high pressure up to 25 GPa and high temperature up to 900°C. The 6-8 type double stage multianvil apparatus was equipped with X-ray diffraction system. A sample was heated in a boron-epoxy octahedral cell, and pressure was calibrated on the basis of the lattice parameters of NaCl and Au. The generated pressure decreased slightly with increasing temperature under the constant load of the press.

The phases of TiO_2 were identified along various routes on the *P-T* diagram. (i) Rutile, the stable phase at ambient conditions, transformed directly to the baddeleyite phase at 12 GPa in the increasing pressure process, and it transformed back to the intermediate α-PbO_2 phase around the same pressure in the decreasing pressure process at room temperature. (ii) the α-PbO_2 phase once formed from rutile by heating at the moderate pressure did not transform to the baddeleyite phase up to, at least, 18 GPa at room temperature, and (iii) the baddeleyite$\leftrightarrow\alpha$-PbO_2 reversible transition was confirmed with the temperature change at pressures higher than 12 GPa. These results give the boundary expressed by the equation, T(°C) = 188.7P(GPa) - 2192.5, between the α-PbO_2 and baddeleyite phases. The rutile$\rightarrow$baddeleyite and the baddeleyite$\rightarrow\alpha$-PbO_2 transitions seems to be explained well by the displacive transition mechanisms proposed by Kusaba et al.

The *P-T* regions, where the two high pressure phases of HfO_2, ortho I and ortho II were formed from the baddeleyite type

phase stable at ambient conditions, were determined by using a microdiffractometer for the recovered samples in addition to the *in situ* diffraction technique. The boundary between the ortho I and ortho II phases lies around 14 GPa at the temperature range between 400°C and 700°C, which is almost the same as that of ZrO_2.

Contents

General Introdution

Many pressure-induced phase transitions in dioxides have been reported hitherto. Especially, high pressure phases of the dioxides with the rutile structure have been of interest in geophysics since they may provide a model for the dense phase of SiO_2. A shock wave experiment for TiO_2 by McQueen et al.[1] in 1967 suggested a phase transition beginning at about 30 GPa. Since then many attempts have been carried out to elucidate the crystal structure of the high pressure phase.[2] Using *in situ* X-ray diffraction technique under high pressure and high temperature, Sato et al.[3] first found that the high pressure phase has the same structure as baddeleyite, the stable phase of ZrO_2 at ambient conditions, but the sample recovered was the mixture of the rutile and α-PbO_2 phases. The stable regions of the three phases on the *P-T* diagram remained as one of the fundamental problems to be clarified.

On the other hand, HfO_2 at ambient conditions has the baddeleyite structure. Bendeliani et al.[4] in 1967 discovered an orthorhombic HfO_2 in the pressure range of 4 ~ 11 GPa and the temperature range of 450~1500°C. In the higher pressure region, Liu[5] in 1980 found that HfO_2 quenched from 16 GPa and about 1000°C possessed an orthorhombic cotunnite structure. However, the phase boundary between these two orthorhombic high pressure phases of HfO_2 has been undetermined, mainly due to the difficulty of the experiments.

In situ X-ray diffraction technique is a very useful tool to study the transitions under high pressure and high tempera-

ture. The process of the successive phase transitions, including unquenchable phases such as the baddeleyite phase in TiO_2, can be clarfied by this method.

In the present paper, the author describes the details of *in situ* X-ray diffraction technique under high pressure and high temperature in Chapter 1 and the phase transitions in TiO_2 and HfO_2 at high pressure and high temperature in Chapter 2 and Chapter 3, respectively.

Chapter 1. *In situ* X-ray diffraction under high pressure and high temperature

§1 High pressure apparatus equipped with X-ray diffractometer

1.1 Pressure generation

As the mutil-anvils can pressurize the sample of large volume and keep stably high-pressure and high-temperature conditions for long time, the "6-8 type" double-stage multianvils were used in the present study. Figure 1-1 is the overall drawing of the hydraulic press by which the multianvils are driven. The upper bolster is fixed and the lower bolster is moved upward by the hydraulic ram. The oil-pressure of the press can be perfectly controlled by a personal computer (NEC 9800). An assemblage of six first-stage anvils made of WC-Co alloy are set in the octahedral hollow formed by joining the upper and lower bolsters as shown in Fig. 1-2. Eight cubic second-stage anvils are set in the cubic space inside the assemblage of the first-stage anvils. When the lower bolster is driven upward by the hydraulic ram, the outer first-stage anvils synchronously moves toward the center of the assembledge, which drives the second-stage anvils toward their center. An octahedral cell is set in the space formed by the triangular faces of the cubic second-stage anvils (Fig. 1-3). The maximum pressure applied to the sample changes largely depending on the material of the second-stage anvils; WC-Co alloy or sintered diamond as described later and on the size of the front faces of the anvils.

1.2 Powder X-ray diffraction by energy dispersive method

In the present *in situ* X-ray diffraction experiment, energy dispersive diffractometry was used due to the anvil geometry. The general picture of the hydraulic press equipped with an X-ray diffraction system is shown in Figs. 1-4 and 1-5.

As shown in Fig. 1-6(a), collimated X-ray beam passes between the 2nd-stage anvils and is irradiated to the sample, and the diffracted X-ray is detected by a solid-state detector (SSD). The incident X-ray, white W radiation, is generated by a rotating-anode type generator (Rigaku, RU-300) with the maximum power of 60kV and 300mA. The SSD (pure Ge) and a multi-channel pulse height analyzer were employed. The SSD can move in the 2θ range of between -29° and +49°. The total system composed of the X-ray generator, collimater, SSD and others in a complete geometrical arrangement is set on the X-Y-Z stage goniometer. The goniometer is placed on the lower plane, on which the lower bolster is placed too. The centering of the sample is performed by the remote contral of the goniometer on which the X-ray system is set.

The three of the 1st-stage anvils are processed so as to have semi-cone slit on their side planes as shown in Fig. 1-6(b); then, the incident and diffracted X-ray beam can pass through the first-stage anvils. The 2θ at which the SSD is set is limited in the range of 0 ~ 15°. The incident and diffracted X-ray beam passes through the gap between the neighboring two second-stage anvils (Fig. 1-7).

§2 Experimental details

2.1 A pressure transmitting medium

The cell in which a sample is included for *in situ* X-ray diffraction under high pressure and high temperature must be transparent to X-ray. Pyrophyllite is the most popular material used as a pressure transmitting medium for the synthesis or physical measurements at elevated temperatures under high pressure because of its thermal insulating properties as well as the favorable mechanical properties. But it cannot be used as the cell material for an X-ray work due to its highly absorbing nature for X-ray radiation. Semi-sintered MgO often used for ultrahigh pressure generation cannot be adopted by the same reason as pyrophyllite. On the other hand, high purity amorphous boron is one of the available materials. It is almost transparent to X-ray with wide range of wavelength because it is a light element. The mechanical strength can be greatly increased by mixing the boron powder with a proper quantity of epoxy resin.

In the present study an octahedral pressure transmitting medium was made of a mixture of amorphous boron and epoxy resin with the weigh ratio of 4:1. The edge lengths of the octahedron were 3.5mm and 5mm for the anvils with the triangular front faces of 1.5mm and 3mm, respectively. The X-ray diffraction pattern of the prepared boron-epoxy octahedron consists of only a few faint halos, which does not so disturbe the diffraction lines of the sample. This medium was used stably without hard troubles under the *P-T* conditions adopted in the present study. The generated

pressure using the boron-epoxy mixture decreased slightly at high temperature due to the thermal expansion of it; the correction was made by using a proper pressure calibrant as described below.

2.2 A cell for X-ray diffraction at high pressure and high temperature

A cell assembly used for the present study is shown in Fig. 1-8. For the difficulty to process the boron and epoxy resin, an octahedron was formed by joining two pyramids. A sample was inserted in the central hole (1.0mm and 2.0mm in diameter, 0.6mm and 1.0mm in depth for the anvils with triangular front faces of 1.5mm and 3.0mm, respectively). A graphite disk heater was selected mainly to insure the X-ray path free from the interference with the heater. A sample was sandwiched between two pieces of heater, the dimensions of which were 1.0mm and 2.0mm in diameter and 0.2mm and 0.4mm in thickness for the anvils of the triangular front faces of 1.5mm and 3.0mm, respectively.

An electric current was supplied to the heater via Mo-electrodes and the temperature was measured using a Pt-Pt13%Rh thermocouple. The junction of the thermocouple was located in the center of the sample and the end of it were led to the outside at ambient conditions. The electric current was supplied from the anvils to the Mo-electrodes in the cell via another Mo-electrode placed on the anvils(Fig.1-9). The temperature drift during 2hr was, for example, within 5°C at 15 GPa and 600°C.

2.3 A path of X-ray beam in the cell

The path of X-ray beam in the cell is shown in Fig. 1-10.

The incident X-ray beam collimated to 0.3 mm in diameter enters the sample cell from its edge. The incident beam and the diffracted beam from the sample passes between the two graphite disk heaters.

§3 Pressure calibration

3.1 Pressure calibration at room temperature

The most commonly used method of pressure measurement is based on the determination of the lattice parameters of some calibrants.Their lattice parameters are converted to the pressures on referring to the pressure-volume relationships confirmed theoretically and/or experimentally.

Sodium chloride (NaCl) is the most popular one of such calibrants; the accurate calculation of the *P-V-T* relation of NaCl was calculated by Decker[6], and its utility has been guaranteed by various experiments. There is no phase transition in NaCl up to 30 GPa, at which the transition to a CsCl structure occurs, and the compressibility of NaCl is relatively large, so that pressure can be determined with a fairly good accuracy from its lattice parameter measurement. On the other hand, the P-V-T relation of gold (Au) was obtained by Jamieson et al.[7] from a shock-wave experiment. Au has been used complementary with NaCl, especially, when some of the diffraction lines of the calibrant overlap with those of a sample.

The mixture of NaCl and Au was used for the pressure cali-

bration at room temperature in the present study. Six diffraction lines of NaCl (200, 220, 222, 400, 420, 422) and five lines of Au (111, 200, 220, 311, 222) were observed at ambient conditions, the 420 of NaCl and 311 of Au overlapped. The pressures were calculated from their lattice parameters on the basis of Decker's NaCl and Jamieson's Au pressure scale at 25°C. The X-ray patterns obtained under increasing pressure generated by the WC-Co alloy anvils with triangular front faces of 1.5 mm are shown in Fig. 1-11 and the relation between the oil - pressure and the generated pressure is plotted in Fig. 1-12. The curve of the pressure calibration obtained by the WC-Co alloy anvils with front triangular faces of 3 mm is also included in Fig. 1-12. Similar calibration was made for the sintered diamond anvils with triangular front face of 1.5mm. The X-ray patterns are shown in Fig. 1-13, and the calibration curve is included in Fig. 1-12, too. We can see the remarkable difference between the two curves by the WC-Co and sintered diamond anvils. In the former, the pressure became almost suturated around 20 GPa due to the plastic deformation of WC-Co alloy, while the pressure increased almost linealy up to, at least, 30 GPa in the later.

When NaCl or Au powder is mixed with a sample, the diffraction patterns became complicated, which made it difficult to observe the appearance of new lines at the onset of the transition in the sample. Therefore, the relations between the oil-pressure and the generated pressure were used for the pressure determination at room temperature in the present study. Only exception is the case for the diffraction experiment of TiO_2 in the decreasing pressure process; Au powder was mixed with TiO_2 as

described later.

3.2 Pressure calibration at high temperature

Although it has been pointed out that internal heating may change the pressure generated in solid-media of high pressure apparatus, the estimations how the internal heating affects the pressure vary largely depending on the nature of the apparatus.

In the present study the P-V-T relation calculated by Decker for NaCl was used in the pressure determination at high temperature too. X-ray diffraction experiments were carried out using the mixture of NaCl and TiO_2 placed between the graphite disk heaters in the octahedral cell (Fig. 1-8). The lattice parameters of NaCl were measured with increasing temperature at intervals of 100°C at three constant oil-pressure of the press. An X-ray exposure time was about 1000 ~ 4000 sec.

For example, the patterns of NaCl and TiO_2 at the oil-pressure of 50 kg/cm^2 and 300°C by using SSD set at $2\theta=13°$ is shown in Fig.1-14. The diffraction lines, 200, 220 and 222, are observed, but the other diffraction lines from TiO_2, the thermocouple and the Mo-electrode appeared; the inner structure of the cell made the profile complicated. For the comparison, the patterns using SSD set at $2\theta=8°$ is given in Fig. 1-15. The only one diffraction line, 200, of NaCl is seen in the all patterns indicating the successive rutile-baddeleyite-type - α-PbO_2 type phase transitions in TiO_2 with increasing temperature. These transitions in TiO_2 are discussed in Chapter 2.

By using these patterns the pressure changes at heating were calculated for three constant oil-pressures corresponding to the pressures of 5, 10 and 15 GPa at room temperature and plotted in Fig. 1-16. The pressure decreases almost linearly with increasing temperature on condition that the press load is kept constant; the pressure at high temperature can be expressed by the equation, $P(GPa) \approx P_0(GPa) - 0.0025T(°C)$, where P and P_0 are the pressure at T and room temperature, respectively. The experiments for identification of the phases of TiO_2 and HfO_2 at high pressure and high temperature were made on the basis of this calibration, by using the cell including TiO_2 or HfO_2 only (not NaCl) in order to avoid the complication of the diffraction patterns, which may result in the misjudgment for the onset of the transition.

Figure Captions

Fig. 1-1 An overall drawing of a hydraulic press.

Fig. 1-2 A cross-section of the "6-8 type" double-stage multianvils set in the press.

Fig. 1-3 The 2nd-stage anvils with triangular front face of 1.5mm and an octahedral cell.

Fig. 1-4 A general picture of the hydraulic press equipped with an X-ray diffraction system.

Fig. 1-5 A photograph of the hydraulic press equipped with an X-ray diffraction system.

Fig. 1-6 Diagram of X-ray diffraction system. (a)X-ray diffraction system, for the double-stage multianvils (in front view) (b)X-ray path through the 1st-stage anvils (in plane view).

Fig. 1-7 X-ray path between the 2nd-stage anvils.

Fig. 1-8 A cell structure for the 2nd-stage anvils with 1.5mm triangular front face.

Fig. 1-9 Arrangment of heating electrodes and a thermocouple for the cell and the 2nd-stage anvils.

Fig. 1-10 Path of X-ray beam in the cell.

Fig. 1-11 X-ray diffraction patterns of NaCl and Au at various pressures and room temperature obtained with WC-Co alloy anvils with 1.5mm front triangular faces.

Fig. 1-12 Pressure calibration curves at room temperature for three kinds of 2nd-stage anvils. White and black symbols represent the results based on the lattice parameters of NaCl and Au, respectively.

Fig. 1-13 X-ray diffraction patterns of NaCl and Au at various pressuresm and room temperature with sintered diamond anvils of 1.5mm front triangular faces.

Fig. 1-14 X-ray diffraction pattern of NaCl and TiO_2 obtained at the oil-pressure of 50kg/cm^2 and 300°C. Unidentified peaks belong to TiO_2, Mo-electrodes and a thermocouple.

Fig. 1-15 X-ray diffraction patterns of NaCl and TiO_2 obtained at the oil-pressure of 50kg/cm^2 and various temperatures. R, α, B and N represent the rutile, α-PbO_2, baddeleyite phases and NaCl, respectively.

Fig. 1-16 Temperature dependence of the generated pressure on heating under three constant oil-pressures of the press. Three line indicate the equation expressed in Text.

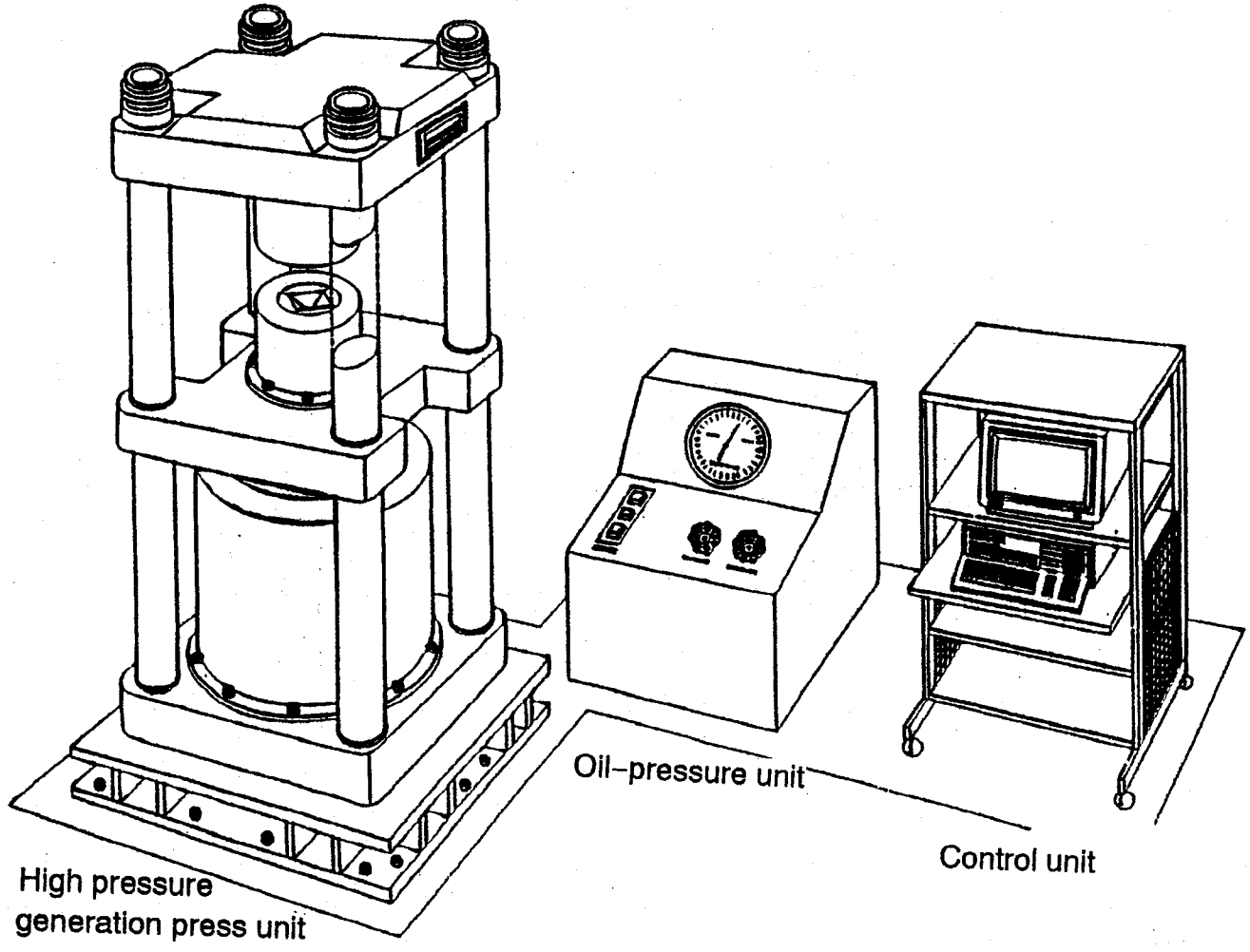
High pressure
generation press unit
Oil-pressure unit
Control unit

Fig.1-1

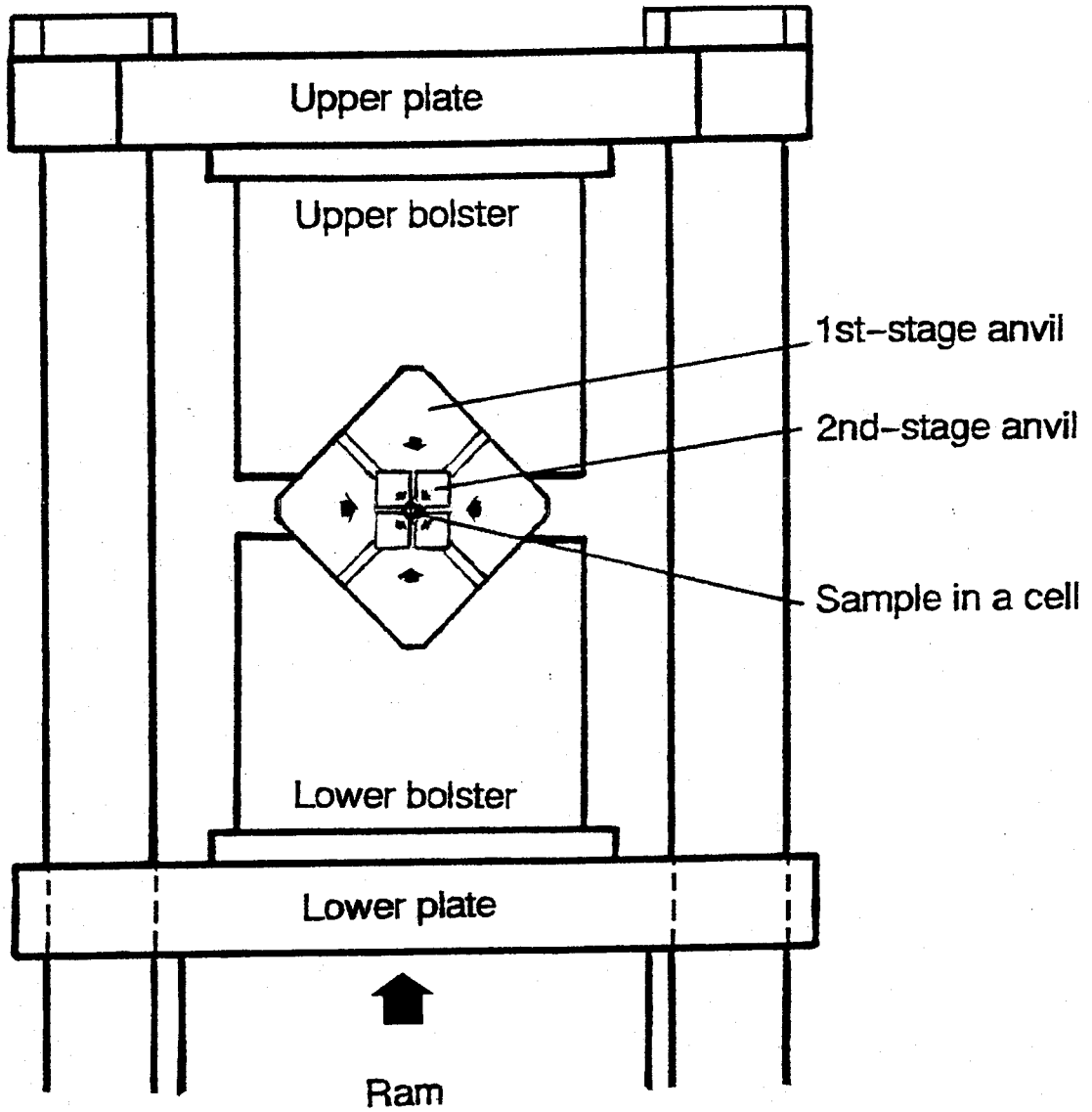
Upper plate
Upper bolster
1st-stage anvil
2nd-stage anvil
Sample in a cell
Lower bolster
Lower plate
Ram

Fig.1-2

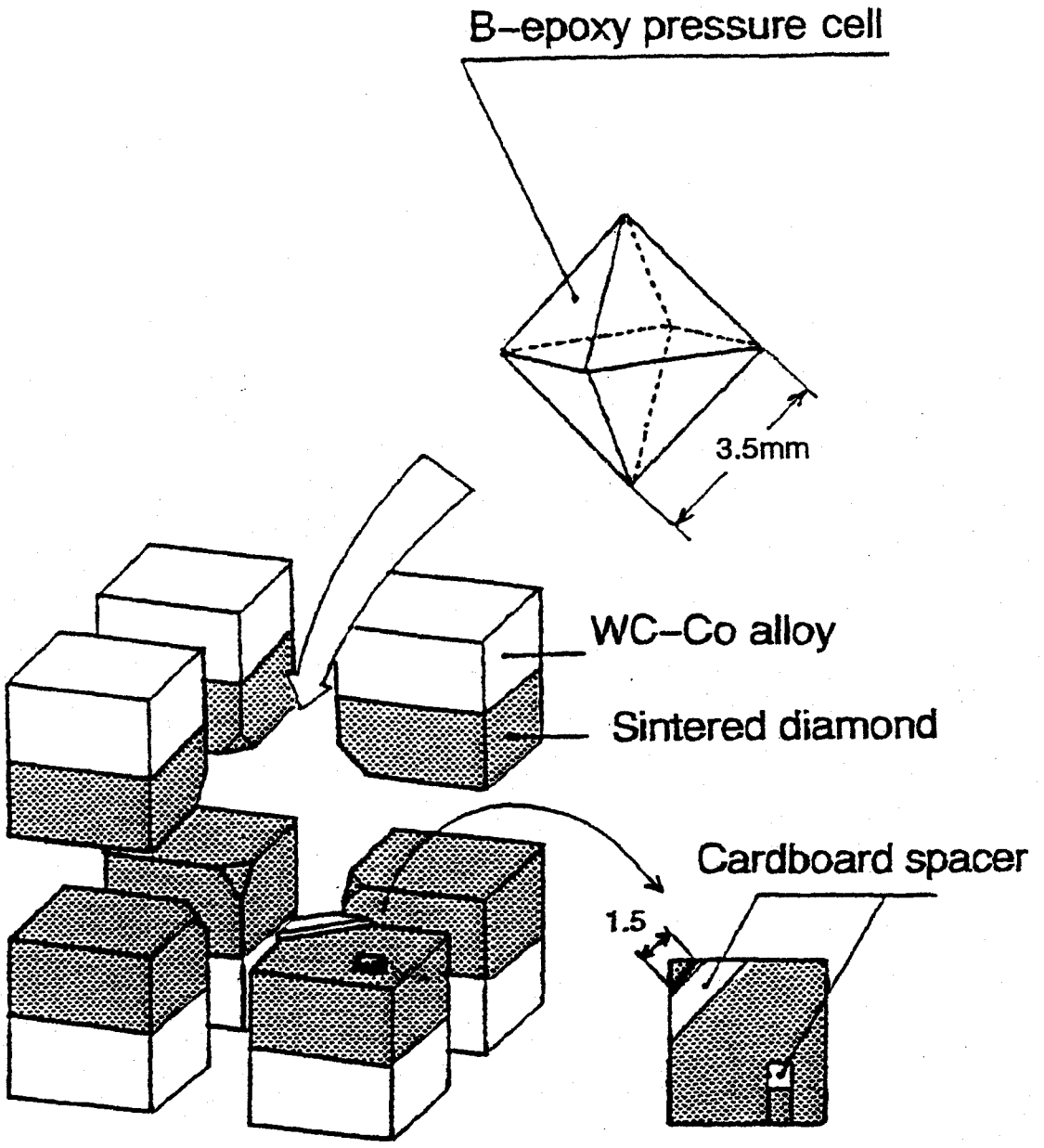
B-epoxy pressure cell
3.5mm
WC-Co alloy
Sintered diamond
Cardboard spacer
1.5

Fig.1-3

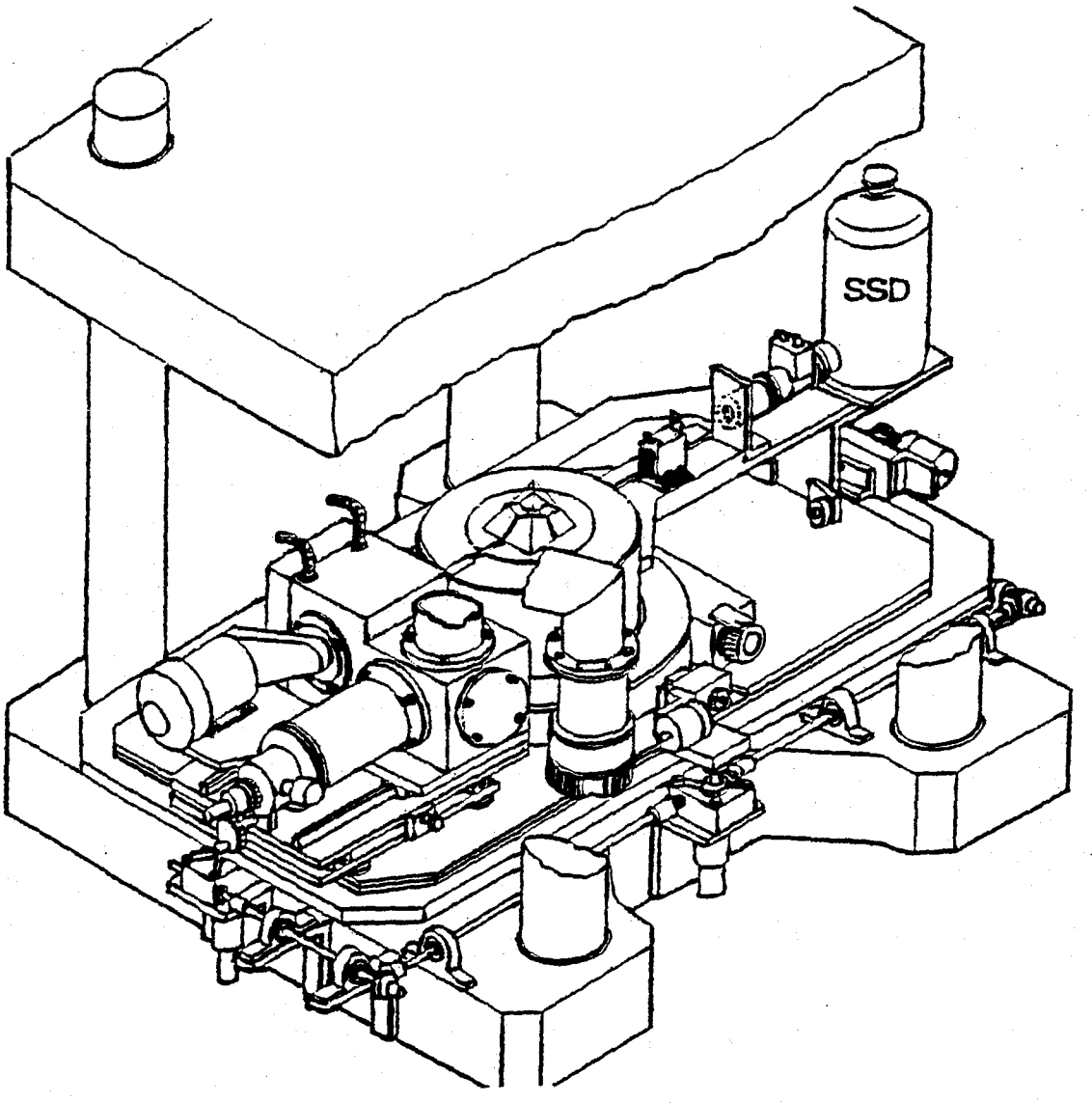

Fig.1–4

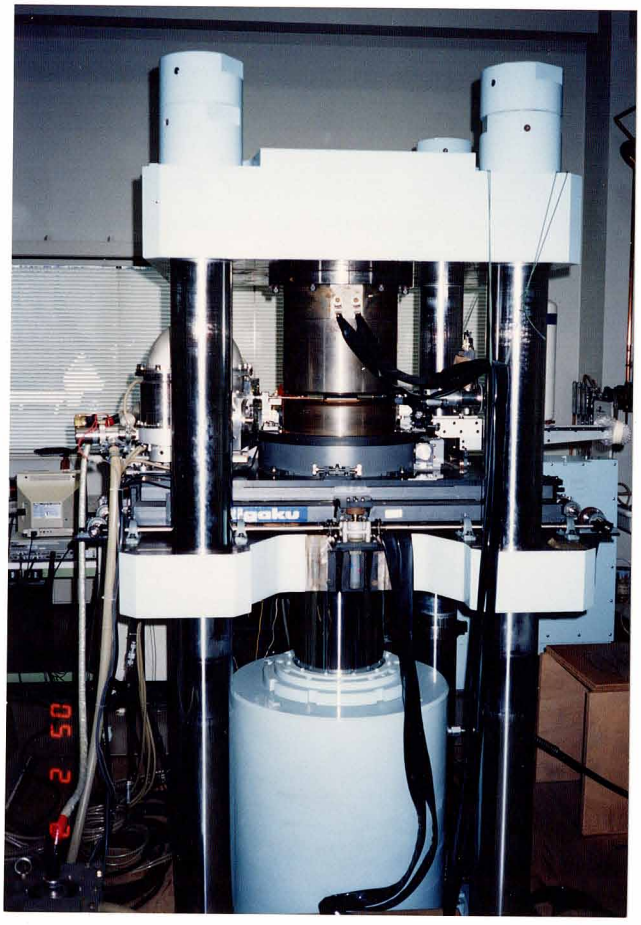

Fig.1-5

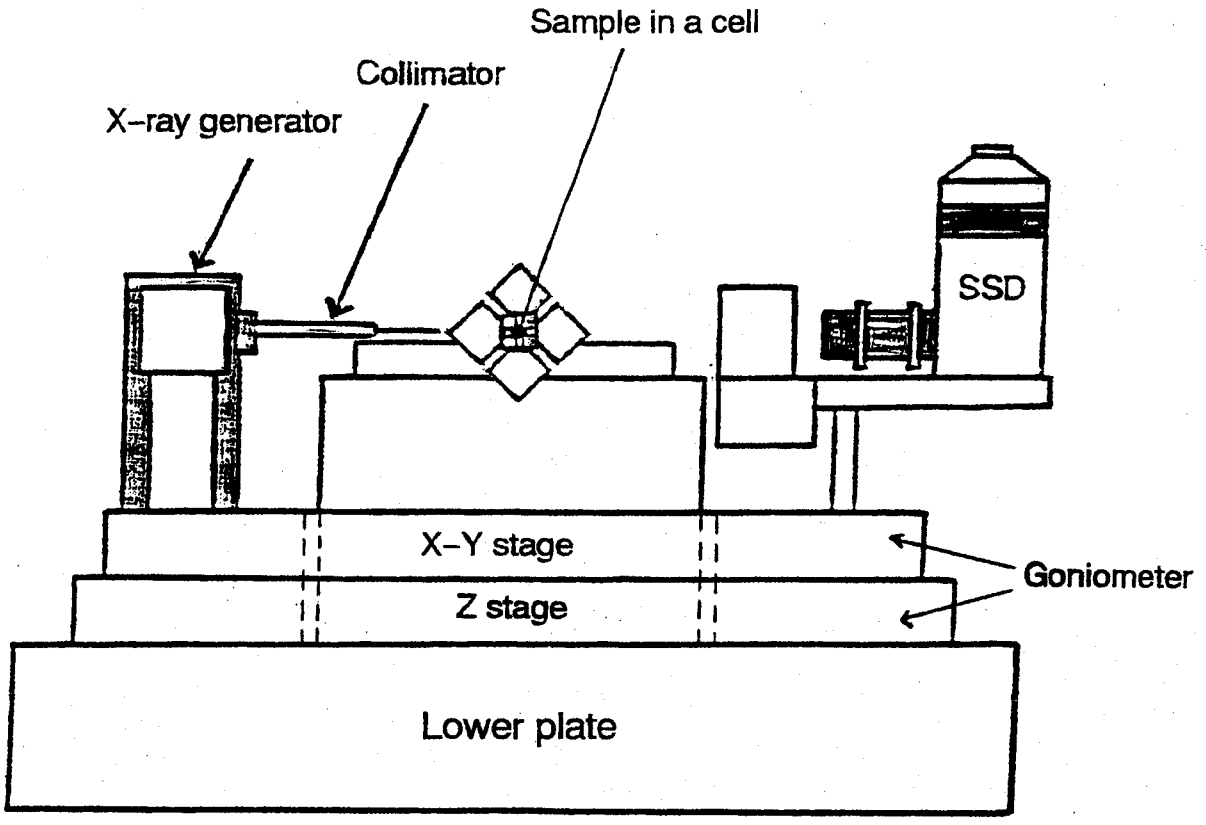
Sample in a cell
Collimator
X-ray generator
SSD
X-Y stage
Goniometer
Z stage
Lower plate

(a)

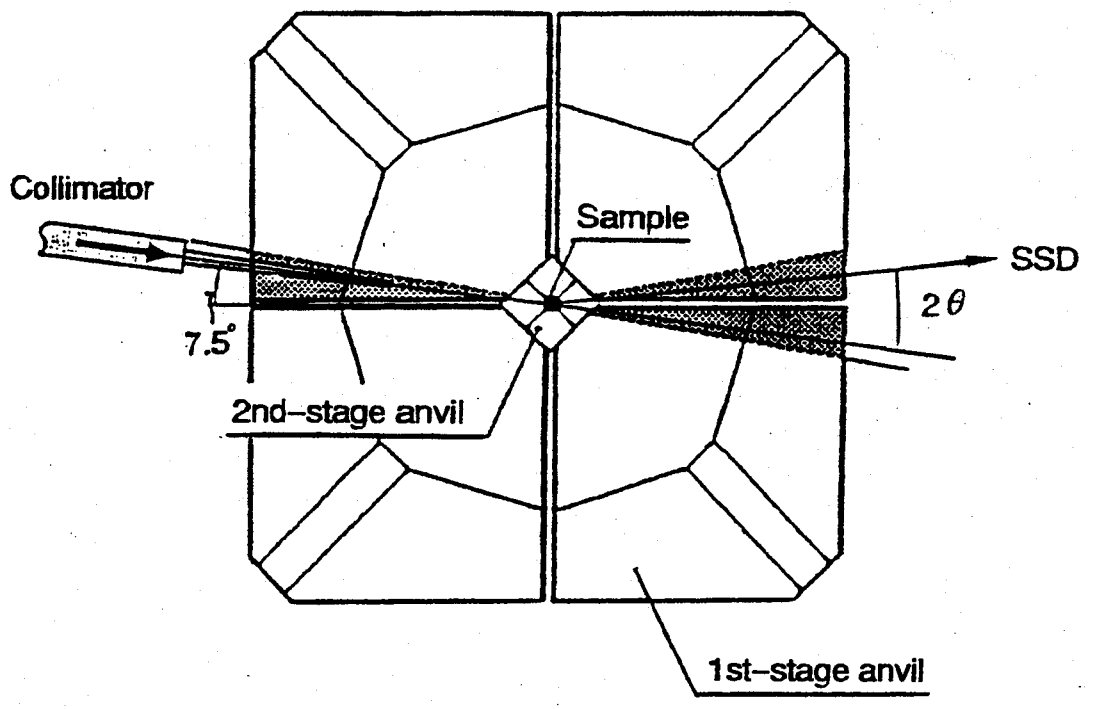
Collimator
Sample
SSD
2θ
7.5°
2nd-stage anvil
1st-stage anvil

(b)

Fig.1-6

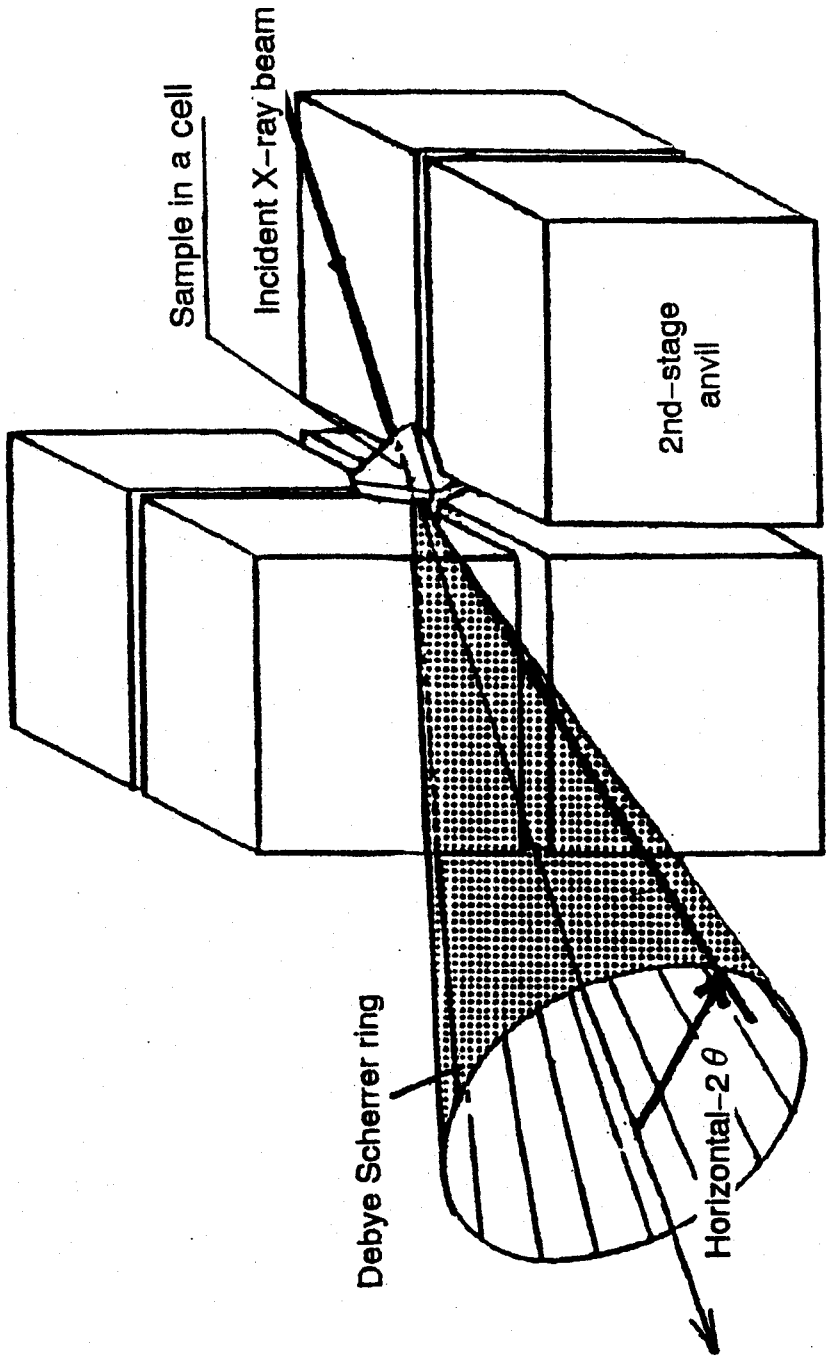
Sample in a cell
Incident X-ray beam
2nd-stage anvil
Debye Scherrer ring
Horizontal-2θ

Fig.1-7

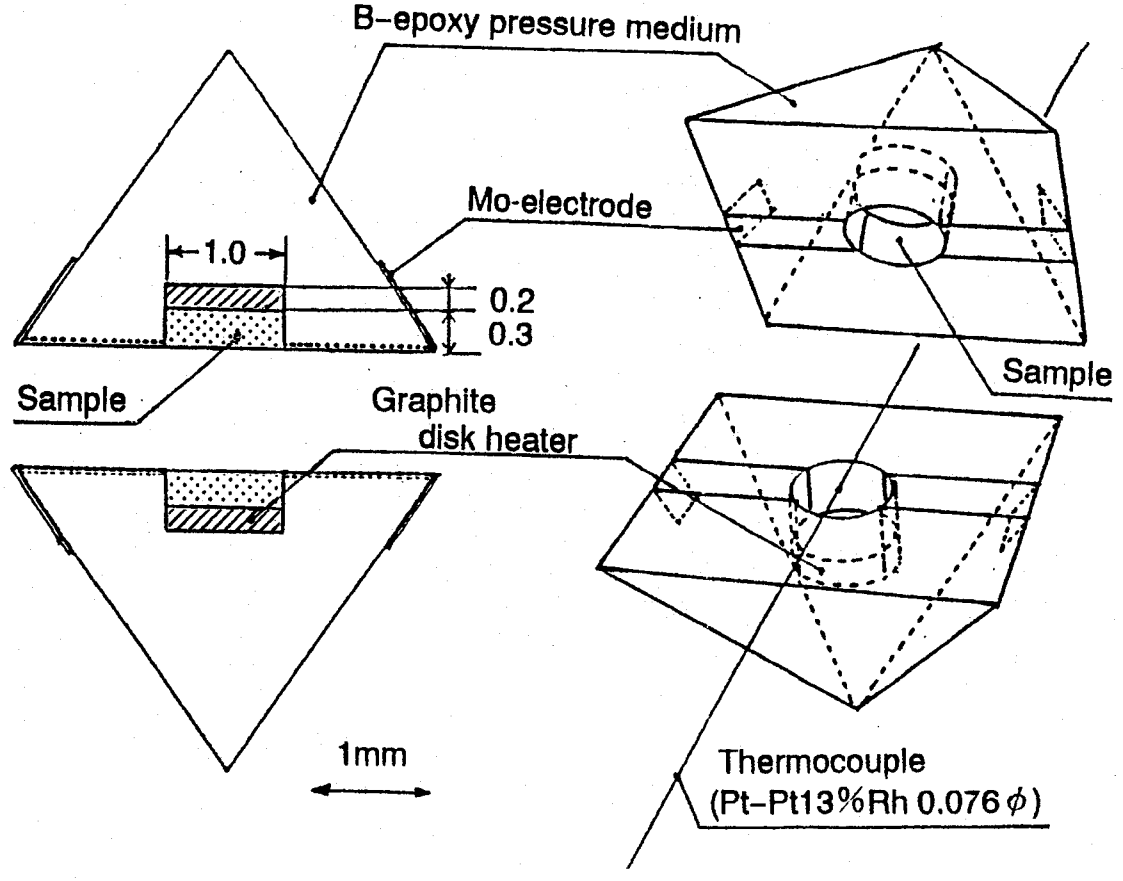
B-epoxy pressure medium
Mo-electrode
1.0
0.2
0.3
Sample
Graphite
disk heater
Sample
1mm
Thermocouple
(Pt-Pt13%Rh 0.076 φ)

Fig.1-8

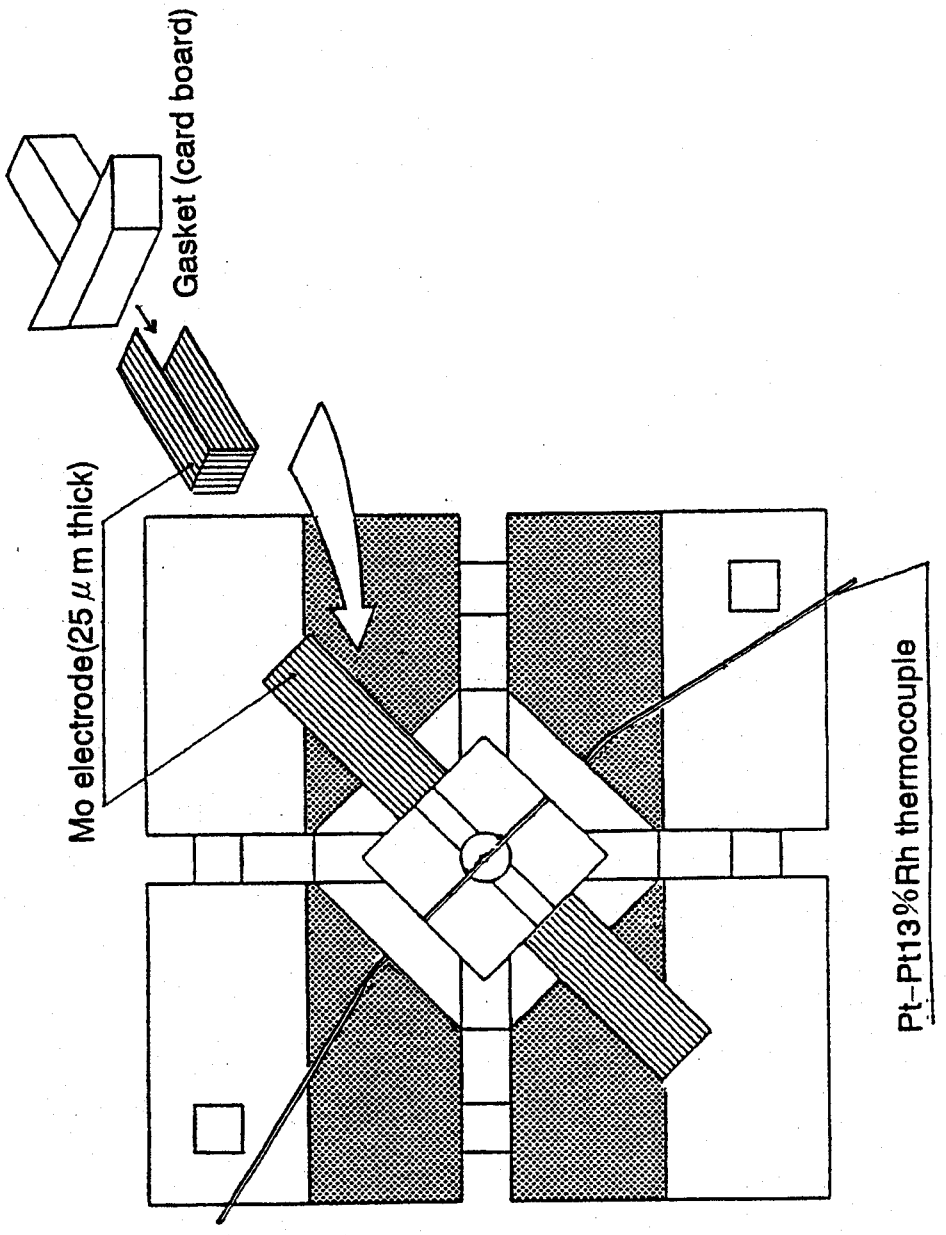
Gasket (card board)
Mo electrode(25 μm thick)
Pt-Pt13%Rh thermocouple

Fig.1-9

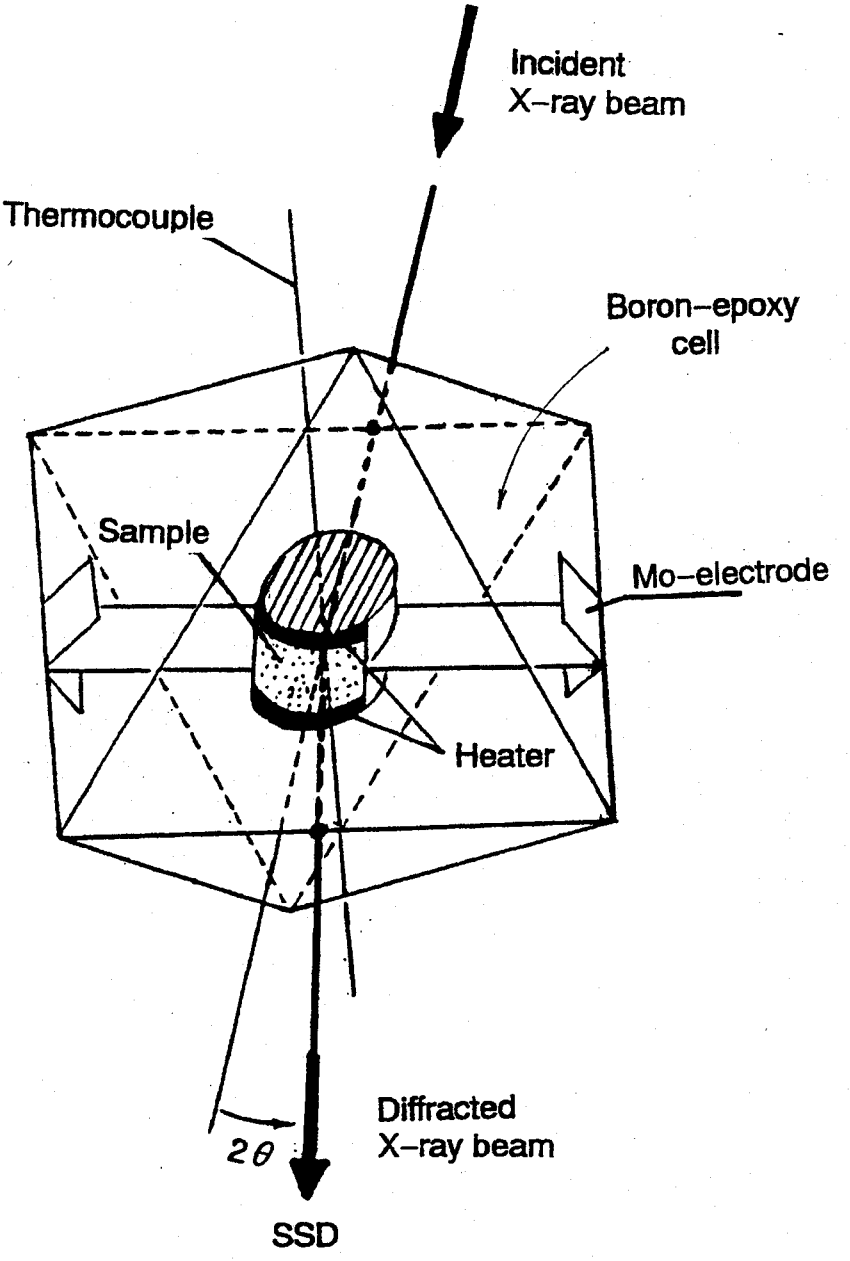
Incident
X-ray beam
Thermocouple
Boron-epoxy
cell
Sample
Mo-electrode
Heater
Diffracted
X-ray beam
2θ
SSD

Fig.1-10

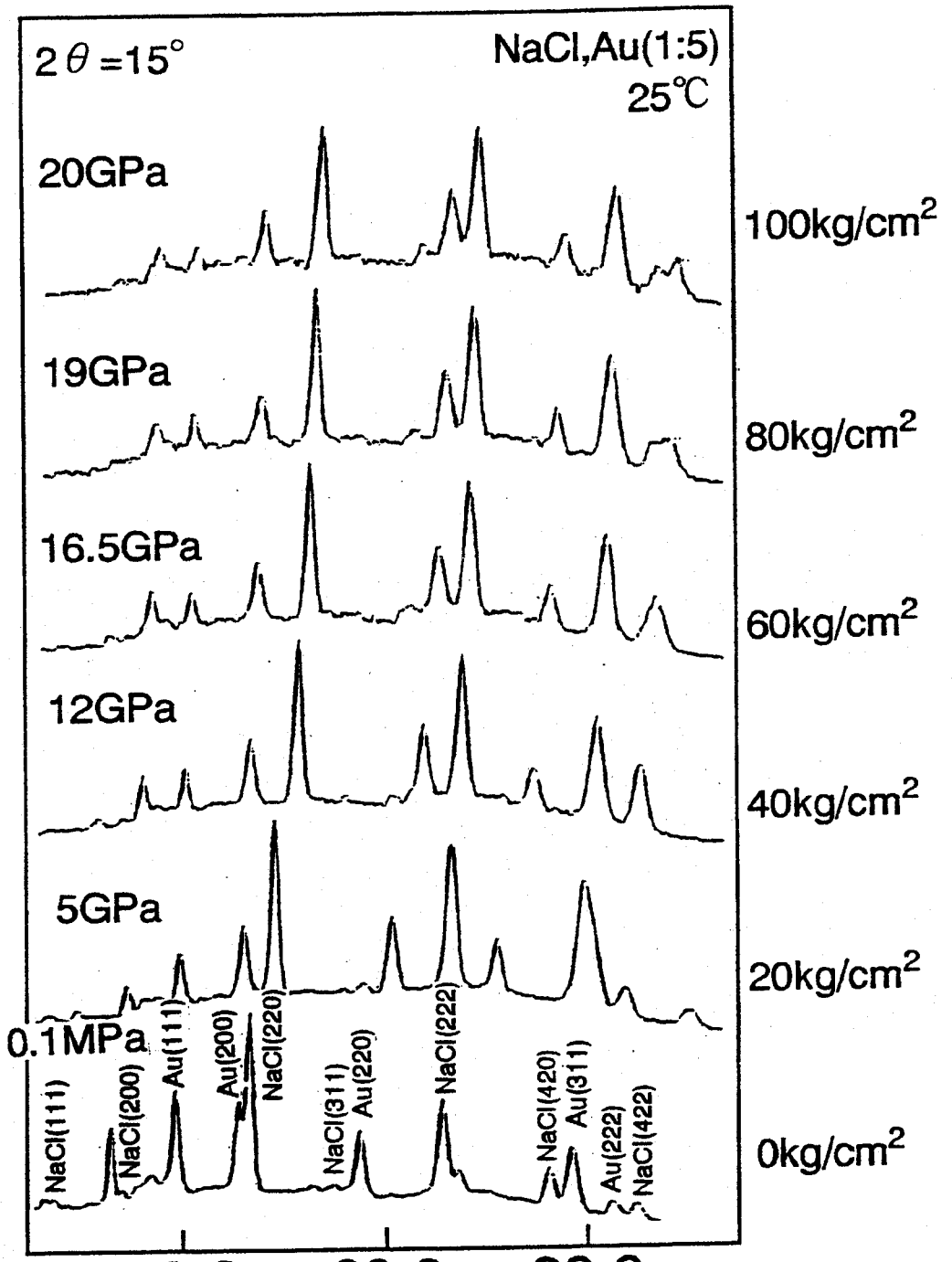
2θ =15°
NaCl,Au(1:5)
25℃
20GPa
100kg/cm²
19GPa
80kg/cm²
16.5GPa
60kg/cm²
12GPa
40kg/cm²
5GPa
20kg/cm²
0.1MPa
0kg/cm²
NaCl(111)
NaCl(200)
Au(111)
Au(200)
NaCl(220)
NaCl(311)
Au(220)
NaCl(222)
NaCl(420)
Au(311)
Au(222)
NaCl(422)
40.0
60.0
80.0
2θ Cu(Kα)
(converted from energy)

Fig.1–11

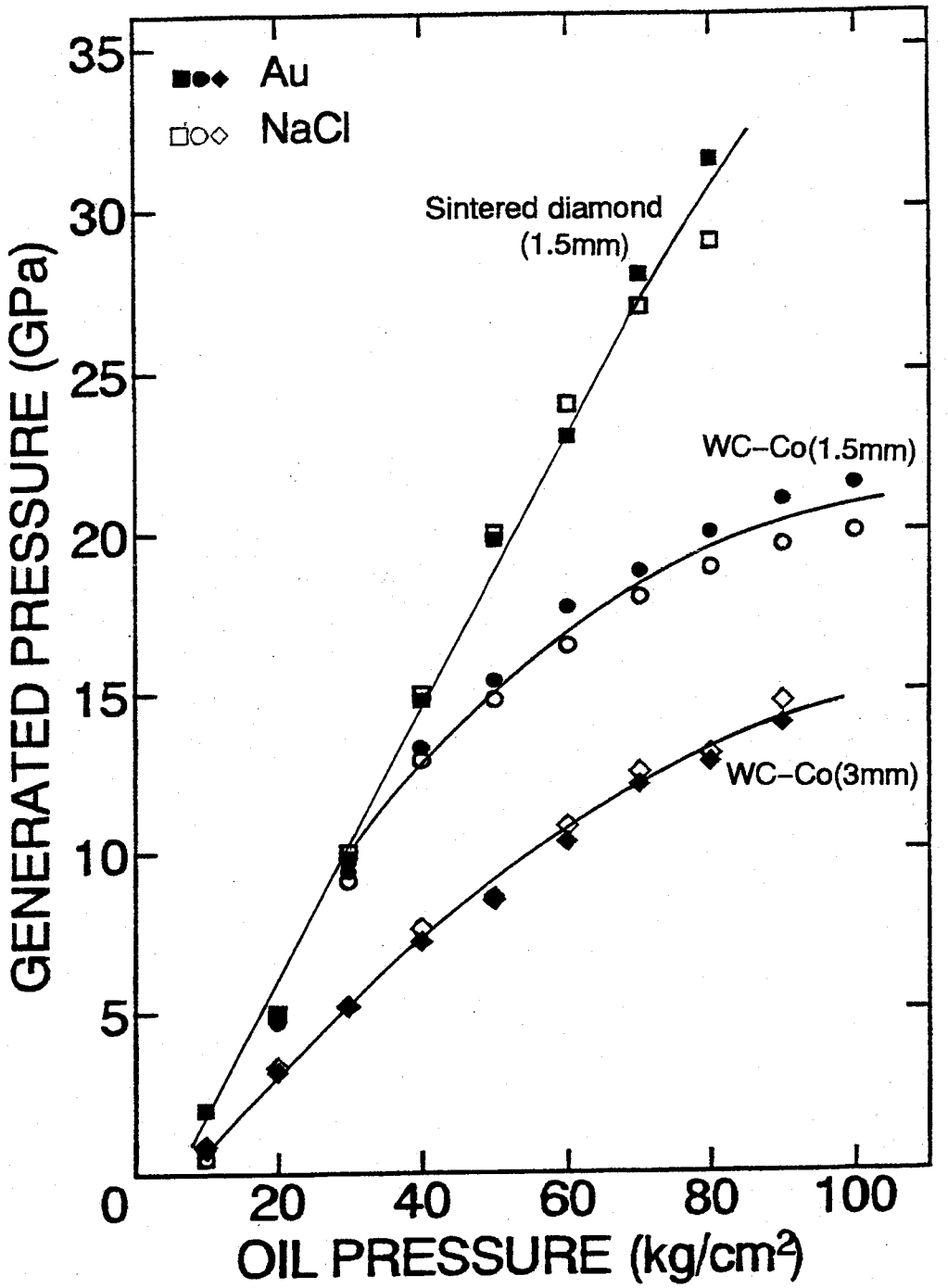
35
30
25
20
15
10
5
0
20
40
60
80
100
■●◆ Au
□○◇ NaCl
Sintered diamond
(1.5mm)
WC–Co(1.5mm)
WC–Co(3mm)
GENERATED PRESSURE (GPa)
OIL PRESSURE (kg/cm²)

Fig.1–12

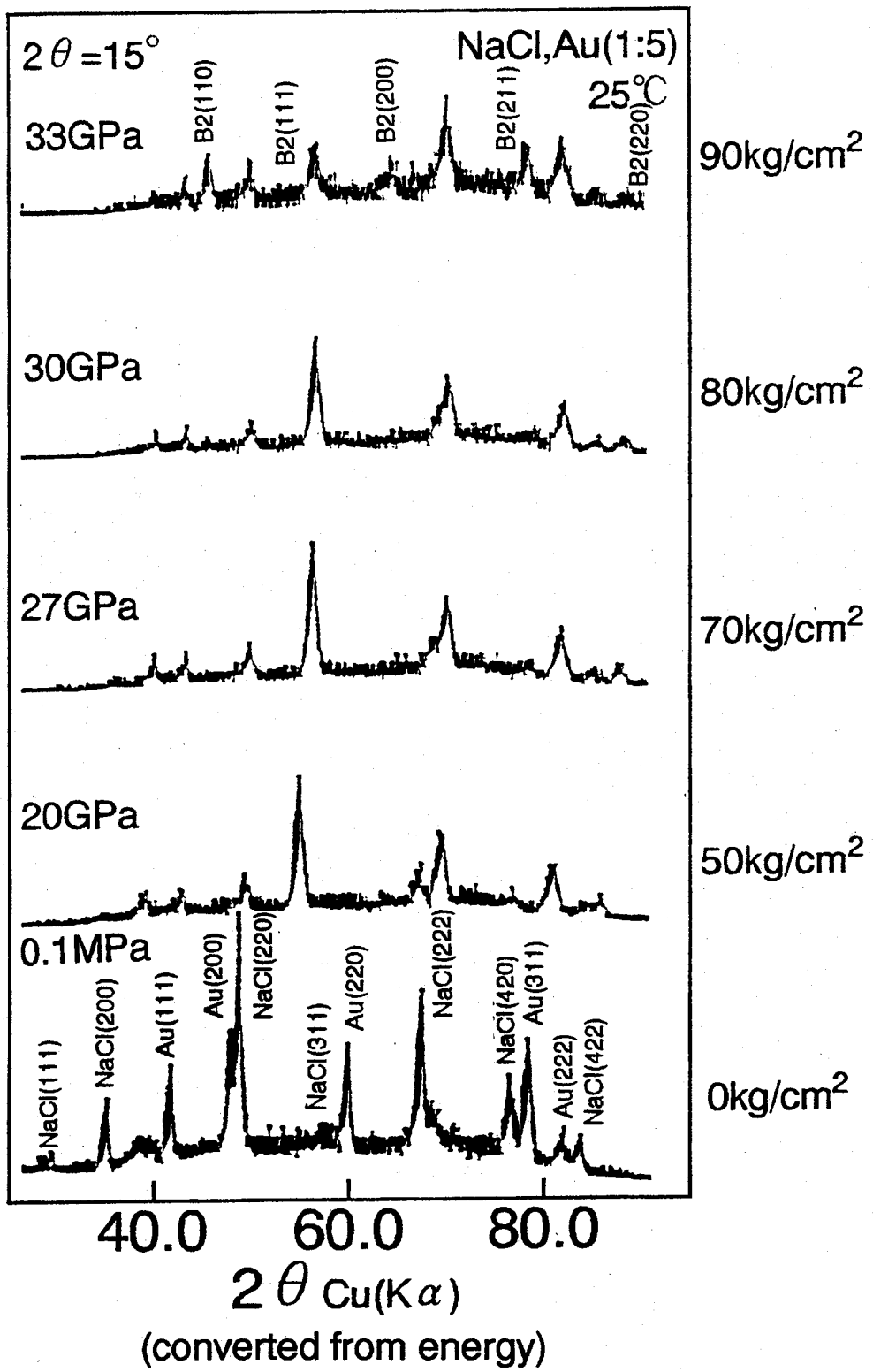
2θ=15°
NaCl,Au(1:5)
25℃
33GPa
B2(110)
B2(111)
B2(200)
B2(211)
B2(220)
90kg/cm2
30GPa
80kg/cm2
27GPa
70kg/cm2
20GPa
50kg/cm2
0.1MPa
NaCl(111)
NaCl(200)
Au(111)
Au(200)
NaCl(220)
NaCl(311)
Au(220)
NaCl(222)
NaCl(420)
Au(311)
Au(222)
NaCl(422)
0kg/cm2
40.0
60.0
80.0
2θ Cu(Kα)
(converted from energy)

Fig.1-13

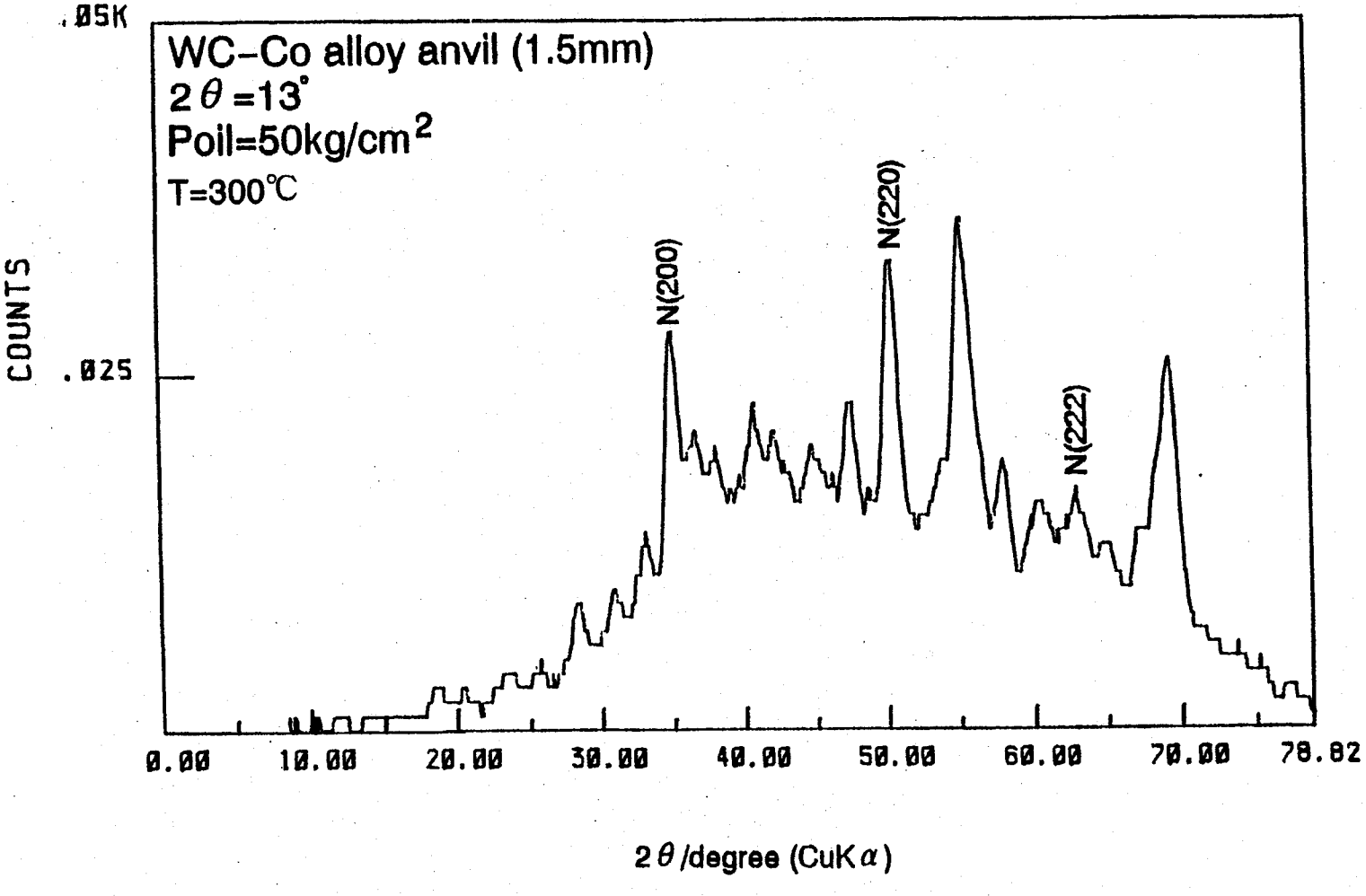
.05K
WC-Co alloy anvil (1.5mm)
2θ=13°
Poil=50kg/cm2
T=300℃
COUNTS
.025
N(200)
N(220)
N(222)
0.00
10.00
20.00
30.00
40.00
50.00
60.00
70.00
78.82
2θ/degree (CuKα)

Fig.1-14

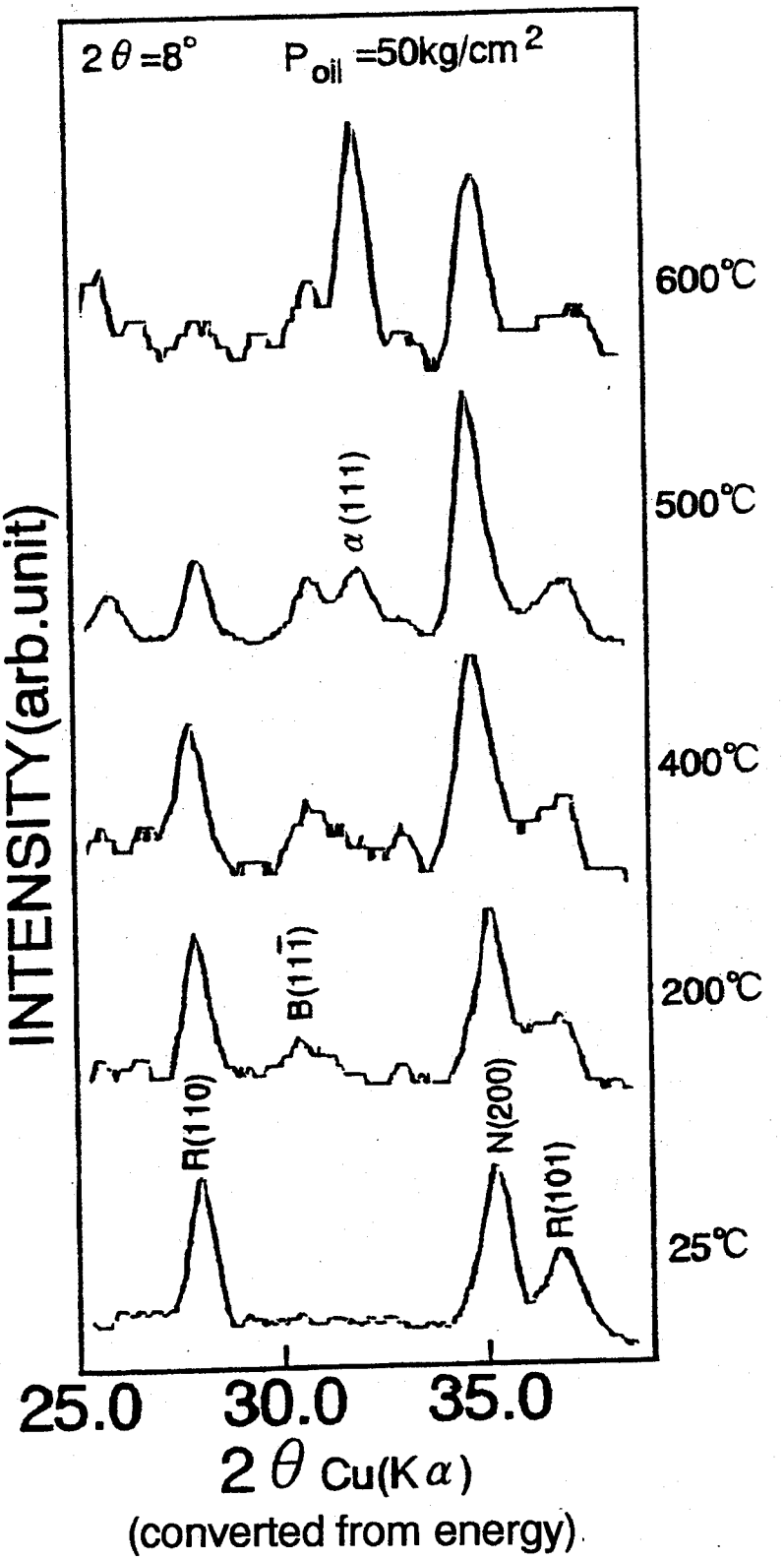
2θ=8°
P oil =50kg/cm 2
600℃
500℃
400℃
200℃
25℃
α(111)
B(11$\bar{1}$)
R(110)
N(200)
R(101)
INTENSITY(arb.unit)
25.0
30.0
35.0
2θ Cu(Kα)
(converted from energy)

Fig.1-15

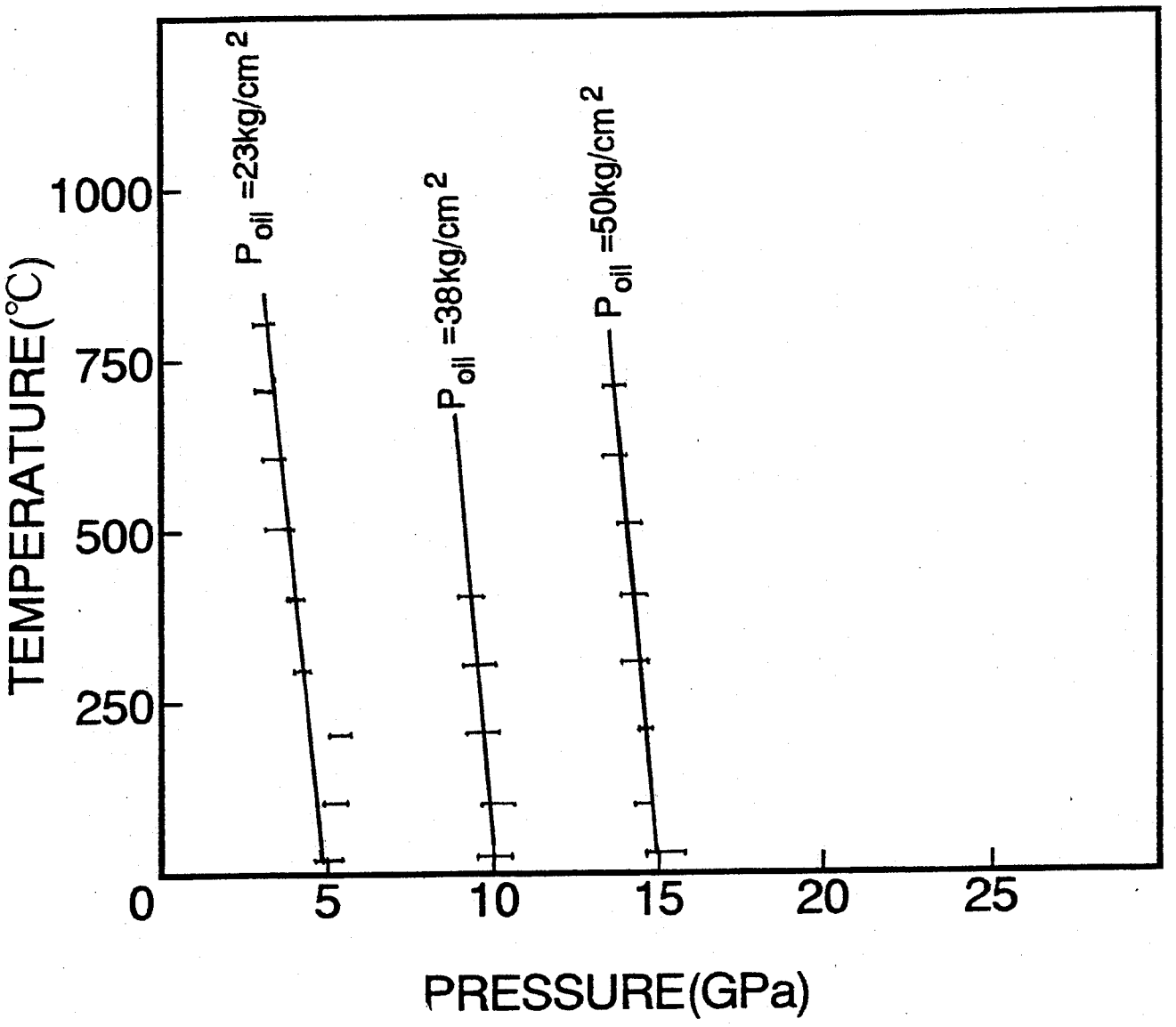
TEMPERATURE(°C)
1000
750
500
250
0
5
10
15
20
25
PRESSURE(GPa)
P_{oil} =23kg/cm^2
P_{oil} =38kg/cm^2
P_{oil} =50kg/cm^2

Fig.1-16

Chapter 2 Phase transitions in TiO_2 at High Pressure and High Temperature

§1 Introduction

Rutile is one of the three polymorphs of titanium dioxide (TiO_2) known to occur in nature. It has a tetragonal structure (space group $P4_2/mnm$) containing two formula units in a unit cell (Fig.2-1(a)). Each Ti^{4+} ion occupies the center of an octahedron formed by six surrounding oxygen ions. The numbers of edges and corners shared by the adjacent octahedra are two and six, respectively(Fig. 2-1(b)). An unusual feature of the rutile structure is the oxygen-oxygen nearest-neighbor distance which is significantly shorter than twice a typical ionic radius of oxygen.

High pressure behavior of rutile has attracted the attention of geophysicists because rutile is a crystal chemical analog of stishovite (SiO_2) and the high pressure study of it may demonstrate polymorphism which could indicate the occurrence of a post-stishovite phase of SiO_2 in the earth's mantle. Many workers have investigated pressure-induced phase transitions in TiO_2 by shock-wave and static pressure experiments.

The high pressure phase of TiO_2 was first quenched from 10 GPa and 500°C by Dachille and Roy[8] in 1962. But, their powder pattern was not indexed due to the small number and poor quality of the diffraction lines, and consequently the structure type was not determined. Bendeliany, Popova and Vereshchagin[9] in 1966 suggested that this phase may have a columbite (α-PbO_2) structure with orthorhombic symmetry (Fig.2-2(a)). In a columbite struc-

ture each Ti atom is octahedrally coordinated by oxygens as well as in rutile, but the face of each octahedron is shared by the adjacent octahedra (Fig.2-2(b)). Jamieson and Olinger[10] found that the rutile phase transforms directly into the α-PbO_2 phase without any intermediate phase in their *in situ* high pressure and high temperature X-ray diffraction studies on TiO_2. They therefore suggested that the α-PbO_2 phase is a stable phase of TiO_2 under high pressure. Mammone et al.[11] in 1980 clarified that the rutile phase transforms directly into the α-PbO_2 phase at ~7GPa by an *in situ* Raman spectroscopy under pressure at room temperature, confirming the previous *in situ* X-ray diffraction study of Jamieson and Olinger[10]. But this transition to α-PbO_2 phase was not observed at room temperature by an X-ray diffraction experiment by McQueen et al.[1] to about 18 GPa, although Ming et al.[12] reported that the α-PbO_2 phase existed at pressure between 9 and 18 GPa at ~1000°C by *in situ* X-ray diffraction using a diamond-anvil cell and a YAG laser for heating. Recently, Akaogi et al.[13] determined accurately the *P-T* boundary between the rutile and α-PbO_2 phases above ~500°C using synchrotron radiation.

On the other hand, the shock-wave studies on TiO_2 (rutile) by McQueen et al.[1] in 1967 indicated the existence of a phase transition accompanied with volume decrease of ~21% at ~35 GPa, which is much higher than the pressure of the above mentioned rutile-α-PbO_2 transition. However, the recovered sample was identified as an α-PbO_2 phase. The fact that the volume of α-PbO_2 type phase is smaller by ~3% than that of rutile, implies that the denser phase observed in the shock wave experiments has yet

to be verified under *in situ* pressure conditions. Mashimo et al.[14] reported that the transition pressure is strongly dependent on the shock-propagation direction. Their results were reconfirmed by Syono et al.[15]. Kusaba et al.[16] proposed a mechanism of the rutile-fluorite phase transition to explain such anisotropic behavior.

A similar transition different from the rutile-α-PbO_2 transition has been also observed in static experiments. By *in situ* X-ray diffraction using a diamond anvil cell and YAG laser heating, Liu[17] obtained the diffraction data indicating a new phase at 25 GPa after heating to 1000°C and tentatively assigned it to a hexagonal phase. However, Ming and Manghnami[12] using the same method reported that the X-ray diffraction data obtained at 20 GPa after heating up to 1000°C indicates the appearance of a new high pressure phase in coexistence with the rutile and the α-PbO_2 phases. They assumed that this new phase has an orthorhombic symmetry. As to Raman spectroscopic technique, Mammone et al.[18] reported that the strongest Raman band assigned to the α-PbO_2 phase disappeared and new peaks appeared at 26 GPa. Because of the low quality of their Raman spectra, they could not determine the structure of the new high-pressure phase.

Recently Sato et al.[19] have studied TiO_2 by *in situ* X-ray diffraction under high pressure and high temperature generated with sintered diamond muitianvils. They reported that the new high-pressure phase begins to appear above ~13GPa at room temperature. The new high-pressure phase coexisted with rutile phase up to 25.0 GPa at room temperature. By heating the sample containing two phases up to 750°C at 20 GPa, the single phase of the high-

pressure phase was formed. They also found that the high-pressure phase formed at 750°C can be quenched to room temperature at 20GPa. They determined by the analysis of the observed diffraction pattern that the new phase has the same structure as baddeleyite, which is the stable phase of ZrO_2 at ambient conditions. The baddeleyite structure is the distorted fluorite structure and the Ti atom is in seven-fold coordination as shown in Fig. 2-3. Recently, Arashi[20] has confirmed this structure by Raman spectroscopic study under high pressure and room temperature.

The previous results on the phase transitions in TiO_2 mentioned above are summarized in Fig. 2-4. Although the formations of the α-PbO_2 and baddeleyite phases have been observed at high pressure and high temperature, the stable *P-T* regions and the nature of the phase transitions are not resolved, because the transition pressure is high and the baddeleyite phase is unquenchable to ambient conditions.

In the present study I intend especially to clarify the phase relations along various *P-T* routes by *in situ* X-ray diffraction technique.

§2 Experimental procedure

The details of the method of *in situ* X-ray diffraction experiments under high pressure and high temperature are described in Chapter 1. The eight cubes of WC-Co alloy with front triangular face of 1.5mm or 3mm edge length were used as the second-stage anvils.

The starting material in the present study was the same as that previously used by Sato et al.[19]. The single crystalline rutile of 99.99% purity (Nakazumi Crystal Laboratory) was crushed and ground into fine powder. Tetragonal unit cell dimensions of the rutile powder were a= 4.5937(7)Å and c=2.9577(6)Å, which gives the unit cell volume of V=62.41(2)$Å^3$ and the X-ray density of 4.250g/cm^3. In order to observe the transition from the α-PbO_2 to the baddeleyite phase, the rutile phase was first converted to the α-PbO_2 phase in the stable *P-T* region of the α-PbO_2 phase and then the α-PbO_2 phase was further compressed.

In the energy dispersive diffraction SSD was set at $2\theta=8°$ and the energy range measurement was from 15KeV to 45KeV. Typical X-ray exposure time was 3000 sec at high pressure and high temperature.

In order to determine the boundary between the *P-T* regions where the α-PbO_2 phase and the baddeleyite phase of TiO_2 exist stable, *in situ* X-ray diffraction experiments were carried out along various routes on the *P-T* diagram. The several typical routes are shown in Fig. 2-5.

The *P-T* conditions where a new phase began to appear or one of the coexisting phases grew up abruptly was considered to belong to the stable region of the phase.

§3 Results

3.1 Rutile → baddeleyite → α-PbO_2 transitions

P increase at room T *P drcrease at room T*

X-ray diffraction patterns for the compression of rutile up to 25 GPa at room temperature, which is represented by the route #1 in Fig.2-5, are shown in Fig. 2-6. X-ray patterns above 15 GPa were obtained with sintered diamond anvils by Sato et al.[21] and those below 14 GPa were obtained with WC-Co alloy anvils in the present study. When the pressure was increased up to 12GPa, the appearance of the $(11\bar{1})$ and (111) lines of the baddeleyite phase was observed. The intensity of these new lines increased with increasing pressure. When the pressure exceeded 20 GPa, the intensity ratio of the old lines and the new lines was reversed, but the rutile phase survived a little still at 25 GPa. During the compression up to 25 GPa the α-PbO_2 phase was not observed at all as described by the previous investigators.

After pressure was released, the mixture of the rutile phase and α-PbO_2 phase (not the baddeleyite phase) was recovered. In order to observe the transitions during the decompression process, *in situ* X-ray diffraction experiment was carried out too. The run was done along the route #2 in Fig. 2-5. At first the single phase with baddeleyite structure was formed by heating at 20 GPa as mentioned later, and then X-ray patterns of it were obtained in the decreasing pressure process at room temperature (Fig. 2-7). In this case the pressure was determined from the lattice parameter of Au powder mixed with the sample on the basis

of Ref.7, since the diffraction line, 200, of NaCl overlapped with the line, 111, of the α-PbO_2 phase. It can be recognized that the α-PbO_2 phase appeared in the pattern at 9.7 GPa and then the baddeleyite phase disappeared completely at 3.1 GPa. The sample recovered to ambient conditions was the α-PbO_2 phase mixed with a small amount of the rutile phase, which is compatible with the results of many shock wave experiments, in which the high pressure phase of the unknown structure has been assumed to convert to the α-PbO_2 phase in the pressure-releasing process.

3.2 Rutile → α–PbO_2 transition
T increase
at high P

As mentioned before, several experimental results have been reported on the transition from the rutile to the α-PbO_2 phase under pressure. Using Raman spectroscopy, Mammone *et al.*[11] observed a small amount of the α-PbO_2 phase at 7 GPa and room temperature and recently Arashi[20] detected the α-PbO_2 phase around 10 GPa and room temperature. However, the apparent transition from the rutile to the α-PbO_2 phase at room temperature was not confirmed by X-ray diffraction technique. Jamieson and Olinger[10] detected it at 10 GPa and 400°C and Akaogi *et al.*[13], who determined the boundary between the rutile and α-PbO_2 phases, described that the transition is very sluggish at temperature lower than 800°C. In the present experiments we did not observe the formation of the α-PbO_2 phase at room temperature, but detected it by heating.

Figure 2-8 shows the patterns corresponding to the following process indicated by the route #3 in Fig.2-5: rutile was compressed up to 8.7 GPa at room temperature and then heated to 565°C, and the pressure was increased again at the constant temperature of 565°C. A little amount of the α-PbO_2 phase was grown at 425°C, but almost the whole rutile phase transformed to the α-PbO_2 phase at 525°C and ~8.7GPa. This is in agreement with the results of the previous studies indicating that the transition from the rutile to the α-PbO_2 phase is very sluggish at low temperature. The recovered sample was completely the α-PbO_2 phase.

3.3 Rutile → baddeleyite → α-PbO_2 transitions

P increase at room T *T increase at high P*

Runs were made along the route #4 in Fig.2-5. At room temperature, as described above, the rutile phase remained up to 12 GPa, where the direct transition to the baddeleyite phase began to occur. The abundance of the formed baddeleyite phase increased with increasing pressure. By heating beyond critical temperatures depending on pressure, both of the baddeleyite and the residual rutile phases disappeared and the α-PbO_2 phase appeared instead. Typical X-ray patterns indicating those transitions are shown in Fig. 2-9. The baddeleyite phase existing at 16.5 GPa transformed completely into the α-PbO_2 phase at 700°C under the same load of the press. Since the generated pressure became lower with increasing temperature under the contant oil pressure of the press as mentioned before, the pressure decreased to 14.8 GPa at 700°C from 16.5 GPa at room temperature. The similar transitions is

also shown in Fig. 1-15 of Chapter 1, in which the sample was the mixture of TiO_2 and NaCl of the weight ratio of 1:3. Since the amount of TiO_2 was small, the baddeleyite phase which usually appeared around 12 GPa at room temperature was not confirmed still at 15 GPa and 25°C as shown in Fig. 1-15.

3.4 α-PbO_2 → baddeleyite transition
P increase
at room T and high T

In order to observe the transition from the α-PbO_2 to baddeleyite phase, the runs along the route #5 in Fig. 2-5 were carried out. First, the α-PbO_2 phase was formed by heating the rutile phase at 12 GPa as shown in Fig. 2-10, and then, the phase transition from the α-PbO_2 to baddeleyite phase was observed to occur or not under high pressure at room temperature. Figure 2-11 shows X-ray patterens in the case that the α-PbO_2 phase was further compressed at room temperature. Although the pressure was increased up to 18 GPa, the α-PbO_2 phase existed still without transforming to the baddeleyite phase. However, when the α-PbO_2 phase was compressed at 450°C along the route #6 in Fig. 2-5, the baddeleyite phase appeared at about 17.3 GPa as shown in Fig. 2-12 and the intensity of the baddeleyite phase increased with increasing pressure.

3.5 Baddeleyite ↔ α-PbO_2 transition
T change
at high P

When the α-PbO_2 phase existing still at 18 GPa at room tem-

perature was heated along the route #7, almost all of the α-PbO_2 phase transformed to the baddeleyite phase at 700°C(Fig. 2-13). Considering that the rutile phase directly transformed to the baddeleyite phase at 12 GPa at room temperature, the α-PbO_2 phase around 18 GPa and room temperature must be a metastable phase; it turned to the stable baddeleyite phase by heating which accelerated the sluggish transition. By further heating to 900°C, the baddeleyite phase transformed to the α-PbO_2 phase, the same transition as mentioned in 3.3. Then, temperature was decreased in order to observe the reverse transition; at 800°C the baddeleyite phase reappeared. We concluded that the equilibrium temperature of the baddeleyite ↔ α-PbO_2 phase transition is about 850°C at 16 GPa. The value of 16 GPa is the corrected pressure for heating.

§4 Discussion

4.1 Phase diagram of TiO_2

The experimental results are summarized in Fig. 2-14, in which the results by previous investigators are also included; the boundary between the rutile phase and the α-PbO_2 phase determined by Akaogi *et al.*[13] and the detections of the formation of the α-PbO_2 phase by Jamieson and Olinger[10], Mammone *et al.*[11] and Ming and Manghnani.[12] The formation of the baddeleyite-type single phase at high pressures and temperatures by Sato *et al.*[3] is also included.

The direct observation of reversible α-PbO_2↔baddeleyite phase transition is, of course, essential for the determination

of the boundary between these two phases. The boundary must pass through the point of 850°C and 16 GPa determined in the present study. However, the α-PbO_2→baddeleyite phase transition is sluggish at low temperature. Instead, 12GPa, the pressure at which the rutile →baddeleyite phase transition was observed at room temperature, was assumed to represent the pressure of the α-PbO_2 → baddeleyite transition as described below. The boundary with the positive slope shown by the straight line in Fig. 2-14 is represented by the equation, T(°C) = 188.7P(GPa) - 2192.5. This is the first example of the boundary determination for the α-PbO_2 type-baddeleyite type phase transition in dioxides.

4.2 On rutile → baddeleyite → α-PbO_2 transitions at room temperature

As mentioned above, the rutile phase directly transformed to the baddeleyite phase, which has one of the fluorite-related type structures, and this high pressure phase was unquenchable and transformed to the α-PbO_2 type phase in the pressure release process. These results are just the same as those observed in the shock-wave experiment. Hyde et al.[22] in 1972 suggested sequential transition of rutile→fluorite→α-PbO_2 phase with only small directional displacements of atoms. Kusaba et al.[16] considered that the transitions can be accomplished by such mechanisms within the short time interval of uniaxial shock compression.

The displacive models proposed by Kusaba et al.[16] for the rutile→fluorite→α-PbO_2 phase transitions seem to be useful in the present study, because the baddeleyite structure is regarded to

be the distorted fluorite structure. The relationships of the crystallographic direction among rutile and fluorite and α-PbO_2 type structure are shown in Table 1, the two equivalent [100] directions in the rutile convert to the [110] and [001] directions in the fluorite structure and the [001] in rutile to $[1\bar{1}0]$ in fluorite at the transition. On the other hand, the three equivalent [100] directions in fluorite convert to [100],[010] and [001] direction in the α-PbO_2 structure the same as that of the rutile→fluorite transition by small atoms displacements. Then the fluorite→α-PbO_2 phase transition may occur in the releasing pressure process.

Comparing the crystal structure of rutile and α-PbO_2, O'Keeffe[23] in 1984 proposed that the packing of O^{2-} in both structures can be considered on the basis of hcp (hexagonal close packing) although, strictly speaking, the packing of O^{2-} in the rutile structure has an intermediate character between hcp and bcc (body centered cubic). However, the positions of Ti^{4+} are very different in these two polymorphs. If the rutile type structure was assumed to transform directly to the α-PbO_2 type structure, the cations have to move considerably in the hcp framework of O^{2-}. It was also experimentally shown in the present study that the transition between the rutile and α-PbO_2 phases required thermal activation energy. Heat treatment for more than 20h at 500°C was necessary for partial conversion of the α-PbO_2 phase TiO_2 to the rutile phase. Therefore, it may be understood that the rutile→baddeleyite transition occurred instead of the rutile→α-PbO_2 transition with increasing pressure at room tem-

perature. This is agreement with the results obtained in the present study.

Thus, the experimental facts at room temperature in the present study that (i) the rutile transformed directly to the baddeleyite phase, not via α-PbO_2 phase, at 12 GPa and (ii) the baddeleyite phase reversed to the α-PbO_2 phase at decreasing pressure between 12.6 and 9.7 GPa, are understood on the basis of the above mentioned mechanism.

4.3 On α-PbO_2 → baddeleyite transition

Although the reversible baddeleyite↔α-PbO_2 transition was observed by thermal cycling around 850°C at 16 GPa, the α-PbO_2 phase at 450°C transformed to the baddeleyite structure at 17.3 GPa, which is much higher than the pressure of the phase boundary in Fig. 2-14. At room temperature, the same transition did not occur up to,at least, 18 GPa. These situations may be expressed in Fig. 2-15, in which the excess pressure for realizing the α-PbO_2→baddeleyite transition in TiO_2 becomes smaller with increasing temperature. The nature of the transition from the α-PbO_2 to baddeleyite phase has not been clear at present. Other realistic features of the transition in TiO_2 observed in the present study are also included in Fig. 2-15.

§5 Conclusion

The present study on the phase transition in TiO_2 at high pressure and high temperature gives the following results:

(1)Rutile, the stable phase at ambient condition, transformed directly to the baddeleyite phase, not via α-PbO_2 phase, at 12 GPa and room temperature.

(2)During the pressure releasing process at room temperature the baddeleyite phase began to transform to the α-PbO_2 phase between 12.6~9.7 GPa, which is similar to the pressure mentioned above, and disappeared around 3 GPa.

(3)The baddeleyite$\leftrightarrow\alpha$-PbO_2 reversible transition was confirmed with the temperature change at high pressure.

(4)The stable P-T regions of the α-PbO_2 and baddeleyite phases were determined, which gives the boundary expressed by the equation, T(°C)=188.7P(GPa)-2192.5.

(5)The rutile → baddeleyite phase transition with increasing pressure and the baddeleyite → α-PbO_2 phase transition with decreasing pressure at room temperature seem to be explained well by the displacive transition mechanisms proposed by Kusaba et al.

(6)The rutile → α-PbO_2 transition was very sluggish below 500°C. This is in agreement with the results by the previous reserchers.

(7)The α-PbO_2 phase once formed by heating rutile at the moderate pressure did not transform to the baddeleyite phase up to, at least, 18 GPa at room temperature. The transition was accomplished by heating at the pressure.

Table 2–1 The relationship of the crystallographic direction among rutile and fluorite and α–PbO_2 type structure proposed by Kusaba et al.[16]

Rutile structure		Fluorite structure		α-PbO_2 structure
[100]	→	[110]or[101]	→	[110]or[101] or[011]
[010]	→	[001]or[010] or[100]	→	[001]or[010] or[100]
[001]	→	$[1\bar{1}0]$or$[10\bar{1}]$ or$[01\bar{1}]$	→	$[1\bar{1}0]$or$[10\bar{1}]$ or$[01\bar{1}]$

Figure Captions

Fig. 2-1 Crystal structure of rutile. (a)the unit cell and (b) the linkage of a TiO_6-octahedron.

Fig. 2-2 Crystal structure of the α-PbO_2 type TiO_2, (a) the unit cell and (b)the linkage of a TiO_6-octahedron.

Fig. 2-3 Crystal structure of the baddeleyite type TiO_2. A titanium atom is in seven-fold coordination.

Fig. 2-4 *P-T* conditions where the three phases of TiO_2 were obsered by previous investigators using the starting material of rutile: the boundary between the rutile and α-PbO_2 phases determined by Akaogi et al.[13], the hatched squares representing the α-PbO_2 phase by Jamieson and Olinger[10], Mammone et al.[11] and Ming and Manghnani[12], and the hatched circles representing the baddeleyite type phase by Sato et al.[3]

Fig. 2-5 Various *P-T* routes along which *in situ* X-ray diffraction were carried out for TiO_2 in the present study.

Fig. 2-6 X-ray diffraction patterns of TiO_2 indicating the formation of the baddeleyite phase from rutile in the increasing pressure process at room temperature along the route #1. The patterns above 15 GPa were obtained by Sato[21] using sintered diamond multianvils. R, B and α indicate the diffraction lines of the rutile, baddeleyite and α-PbO_2 phase of TiO_2, respectively.

Fig. 2-7 X-ray diffraction patterns of TiO_2 in the decreasing pressure process at room temperature along #2. The transition from the baddeleyite to the α-PbO_2 phase

was confirmed at 9.7 GPa.

Fig. 2-8 X-ray diffraction patterns of TiO_2 in the heating process at ~8.7 GPa and then increasing pressure process at 565°C along #3. The α-PbO_2 phase formed at 425°C existed still in such *P-T* conditions.

Fig. 2-9 X-ary diffraction patterns of TiO_2 in the heating process at ~16.5 GPa along #4. The rutile → baddeleyite → α-PbO_2 transitions were confirmed. The pressure decreased to 14.8GPa at 700°C when the oil pressure was kept constant (see Text).

Fig. 2-10 X-ray diffraction patterns of TiO_2 indicating the formation of the α-PbO_2 phase from rutile at 12 GPa and 525°C.

Fig. 2-11 X-ray diffraction patterns of TiO_2 indicating no further transition from the α-PbO_2 type phase in the increasing pressure process at room temperature along #5.

Fig. 2-12 X-ray diffraction patterns of TiO_2 indicating the transition from the α-PbO_2 to the baddeleyite phase in the increasing pressure process at 450°C along #6.

Fig. 2-13 X-ray diffraction patterns of TiO_2 in the increasing and then decreasing temperature processes at ~18 GPa. The metastable α-PbO_2 phase transformed to the baddeleyite phase and then transformed again to the stable α-PbO_2 phase by heating, which was reversed to the baddelayite phase by cooling. The equilibrium conditions of 16.5 GPa and 800°C were obtained for the reversible baddeleyite ↔ α-PbO_2 transition.

Fig.2-14 Phase diagram of TiO_2. The boundary between the α-PbO_2 and baddeleyite phases determined in the present study is represented by the equation, T(°C) = 188.7P(GPa)-2192.5. The boundary between the rutile and α-PbO_2 phases and the formations of the α-PbO_2 and baddeleyite phases (hached symbols) obtained by the previous investigators are also included.

Fig. 2-15 The diagram represents the sluggish phase transitions in TiO_2 observed at relatively low temperature. The phase boundary between the α-PbO_2 and baddeleyite phases determined in the high temperature region passes through the baddeleyite → α-PbO_2 transition points at the lower temperatures and the rutile → baddeleyite transition point at room temperature, which may be understood on the basis of the transition mechanisms proposed by Kusaba et al.[16] (see Text).

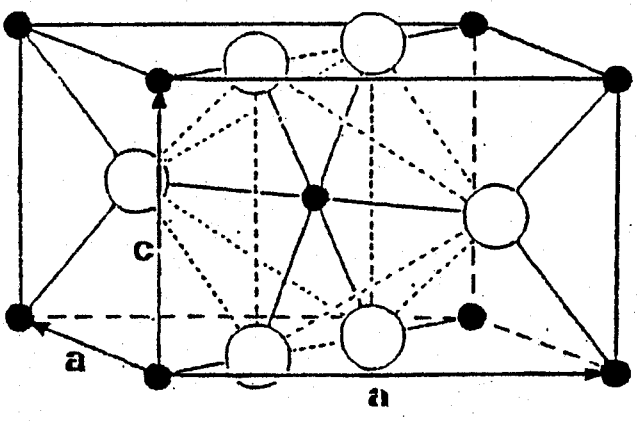

(a)

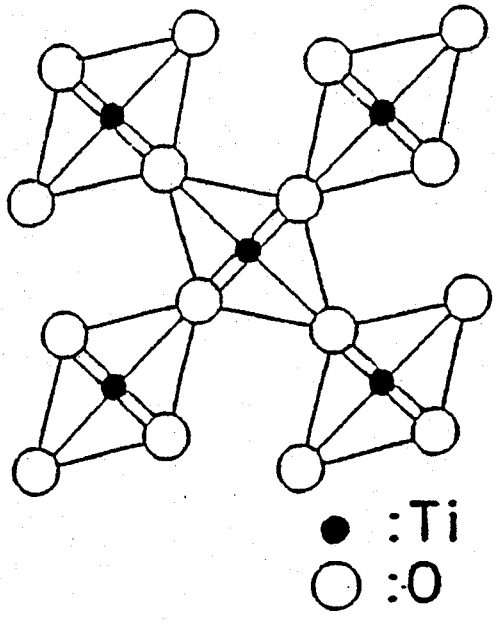

(b)

Fig.2–1

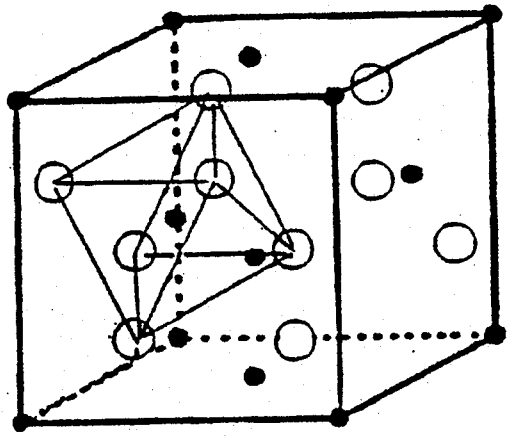

(a)

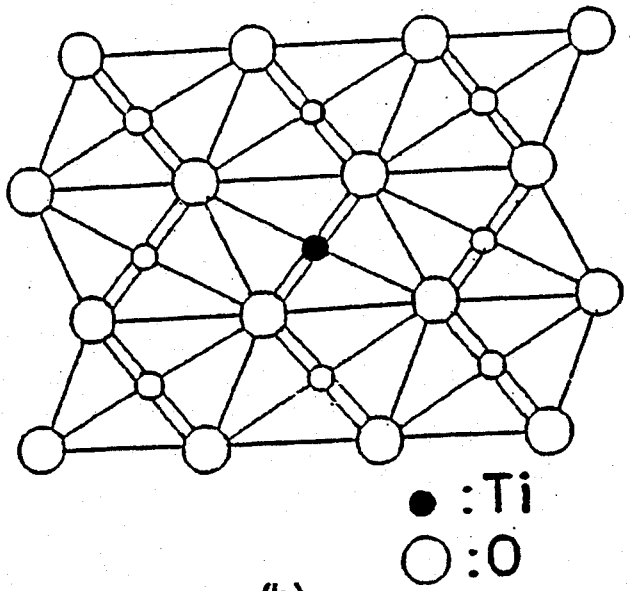

(b)

Fig.2-2

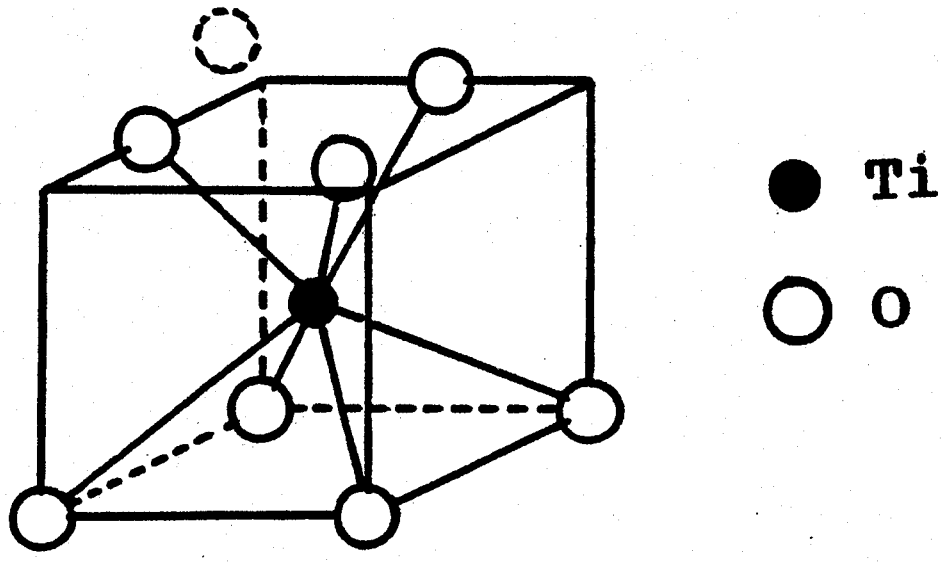

Fig.2–3

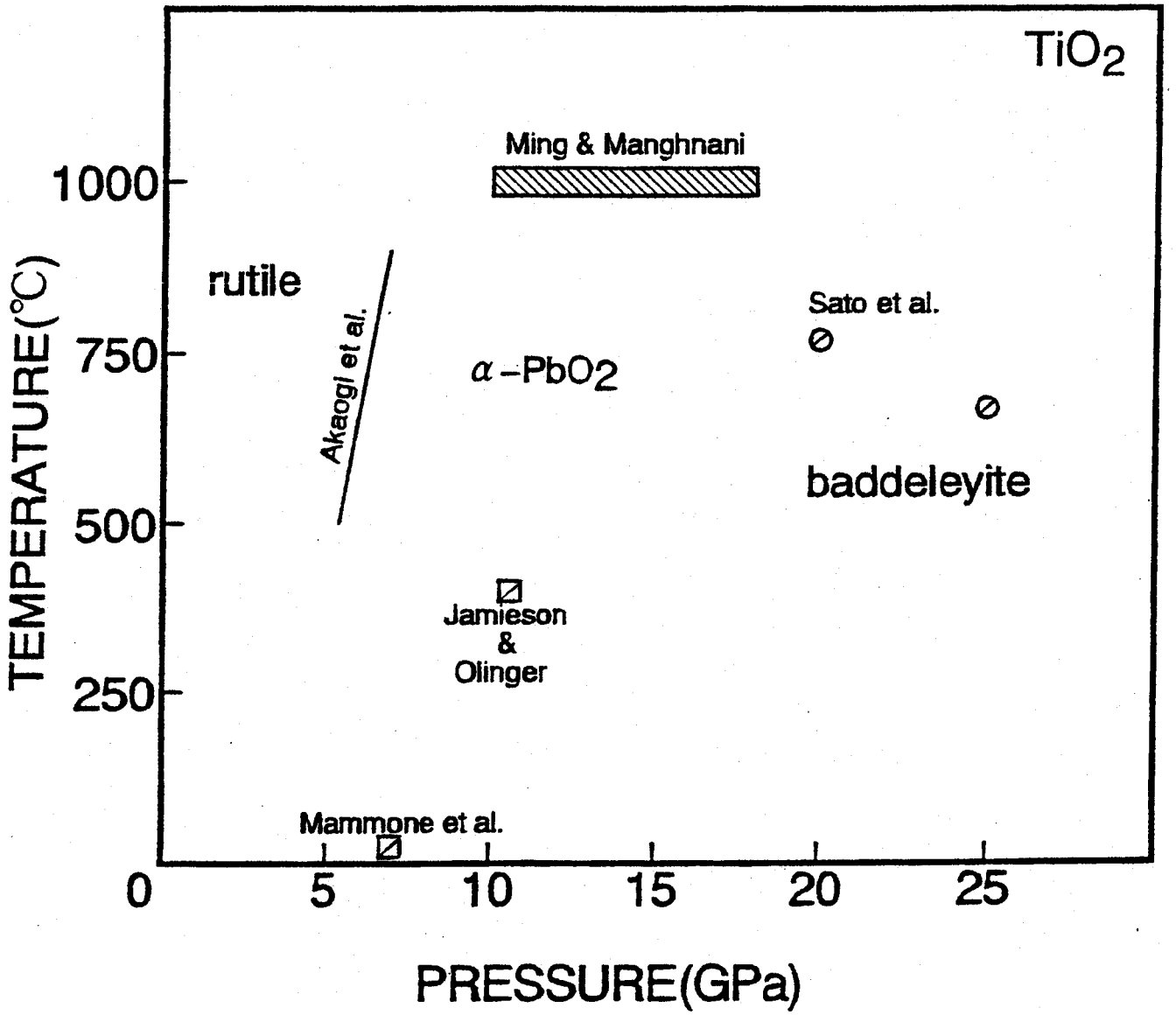
TiO2
Ming & Manghnani
1000
rutile
Akaogi et al.
Sato et al.
750
α-PbO2
baddeleyite
500
Jamieson
&
Olinger
250
Mammone et al.
0
5
10
15
20
25
TEMPERATURE(°C)
PRESSURE(GPa)

Fig.2-4

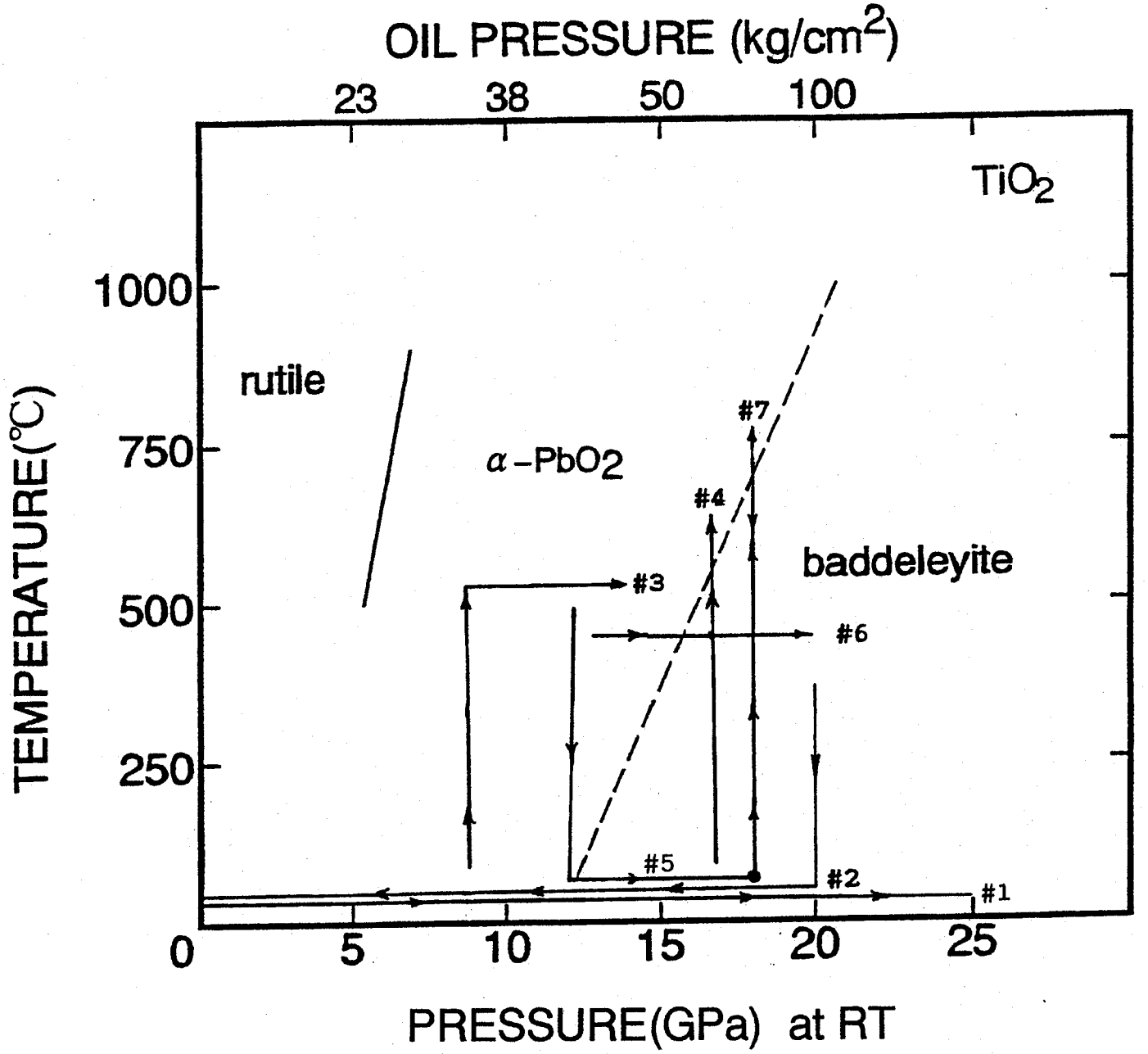
OIL PRESSURE (kg/cm2)
23
38
50
100
TiO2
1000
750
500
250
0
TEMPERATURE(°C)
rutile
α-PbO2
baddeleyite
#1
#2
#3
#4
#5
#6
#7
5
10
15
20
25
PRESSURE(GPa) at RT

Fig.2-5

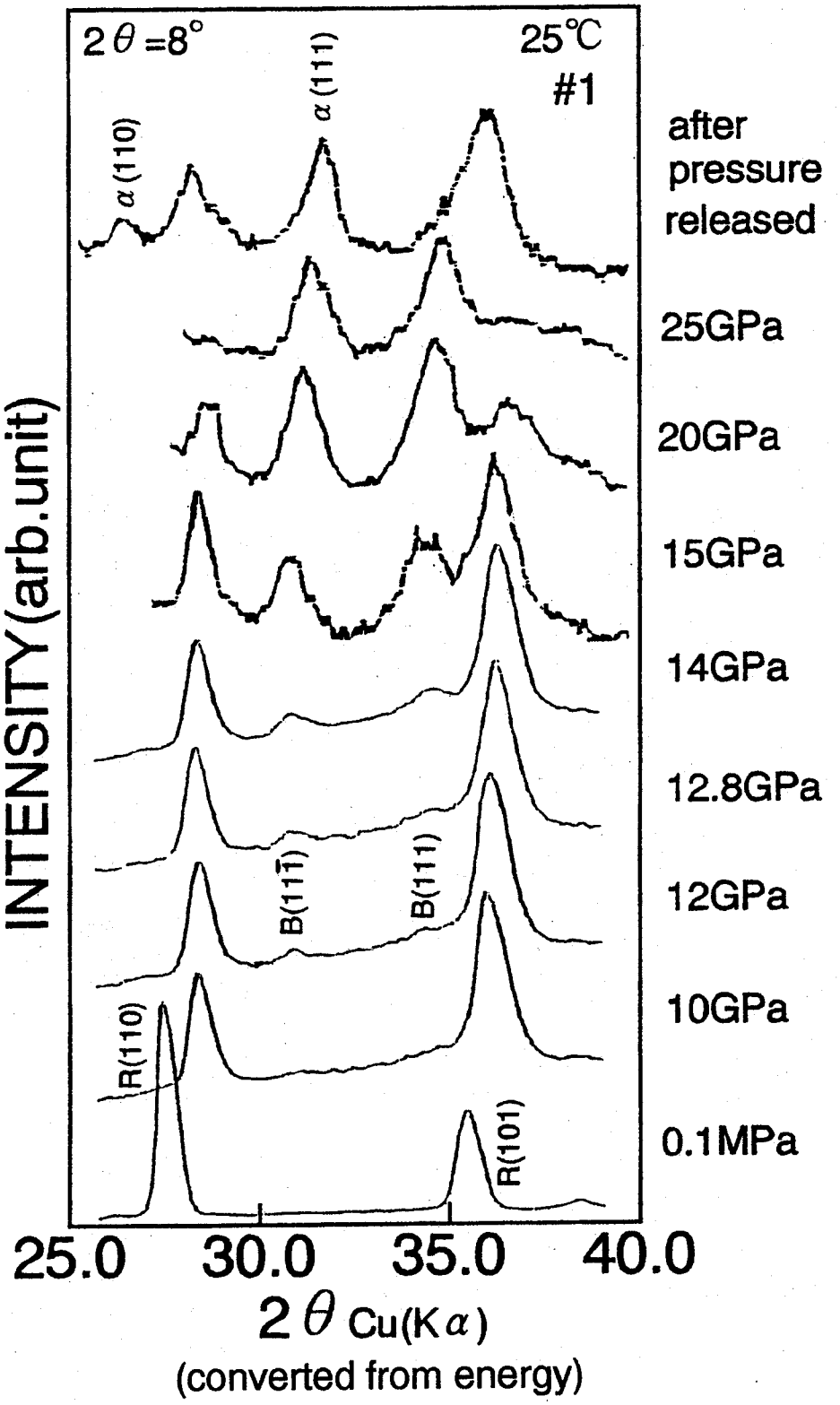
2θ=8°
25℃
#1
α(110)
α(111)
after pressure released
25GPa
20GPa
15GPa
14GPa
12.8GPa
12GPa
10GPa
0.1MPa
B(11$\bar{1}$)
B(111)
R(110)
R(101)
INTENSITY(arb.unit)
25.0
30.0
35.0
40.0
2θ Cu(Kα)
(converted from energy)

Fig.2–6

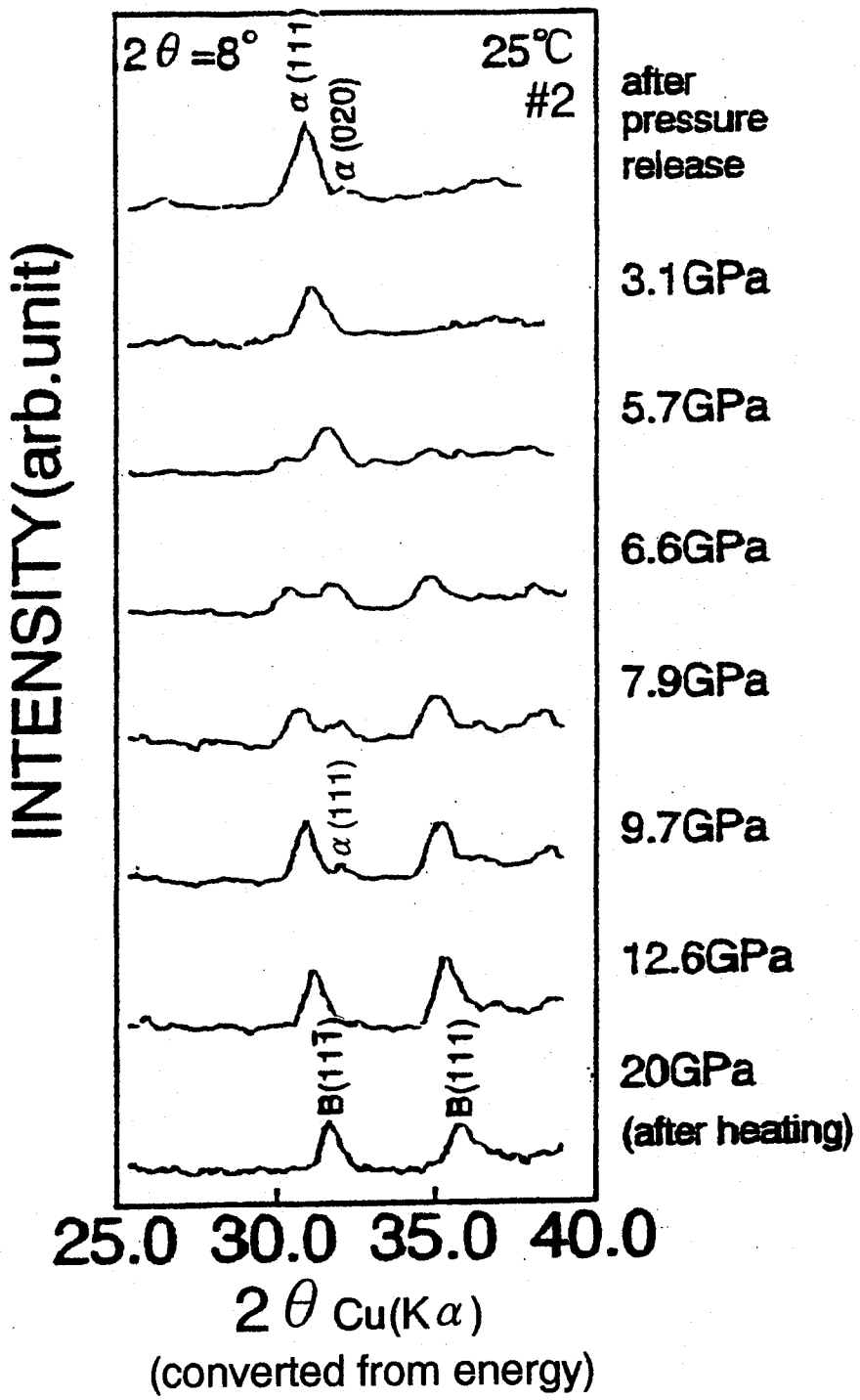
2θ =8°
25℃
#2
α (111)
α (020)
after pressure release
3.1GPa
5.7GPa
6.6GPa
7.9GPa
α (111)
9.7GPa
12.6GPa
B(11$\bar{7}$)
B(111)
20GPa
(after heating)
INTENSITY(arb.unit)
25.0 30.0 35.0 40.0
2θ Cu(Kα)
(converted from energy)

Fig.2–7

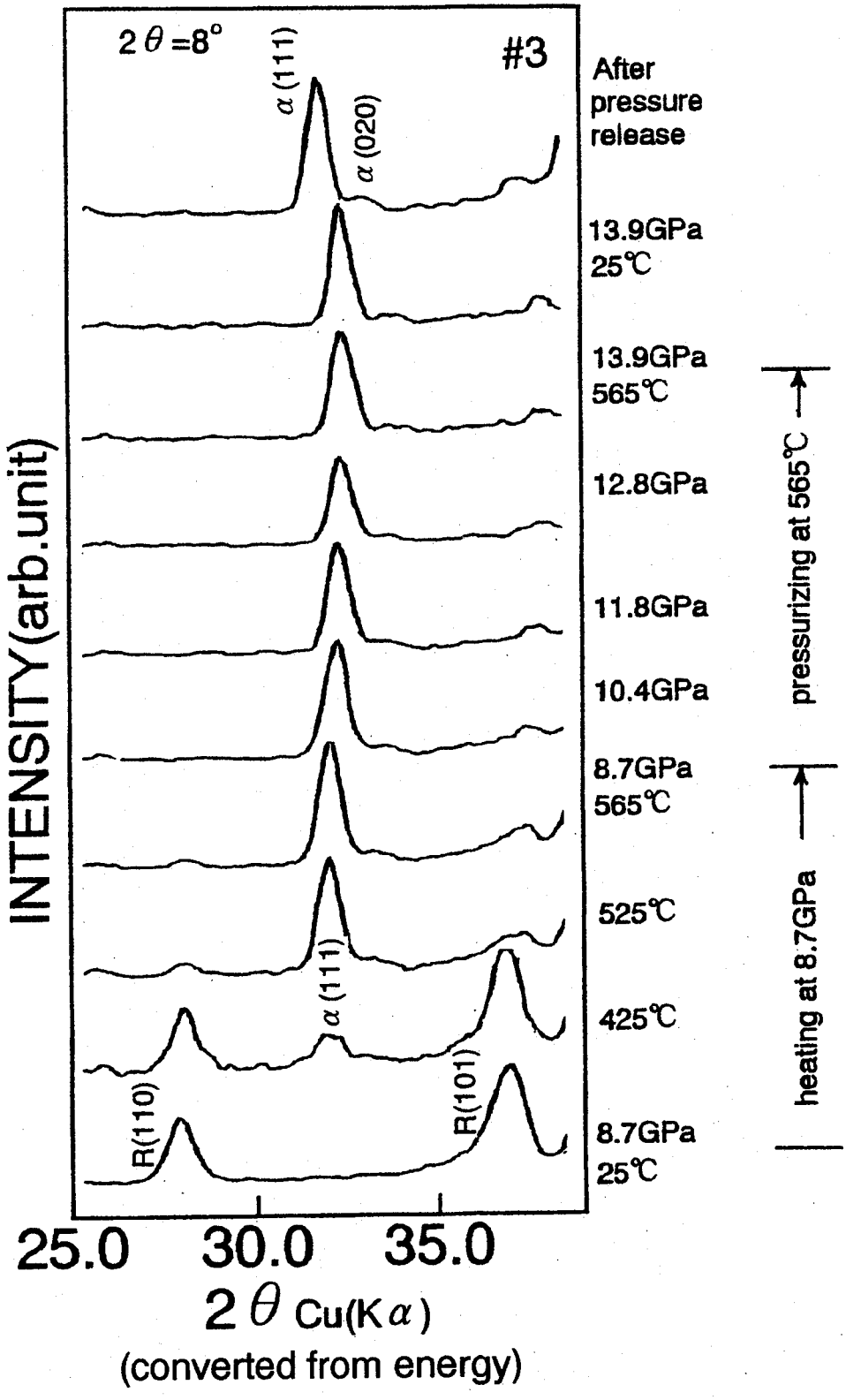
2θ=8°
#3
α(111)
α(020)
After pressure release
13.9GPa 25℃
13.9GPa 565℃
12.8GPa
11.8GPa
10.4GPa
8.7GPa 565℃
525℃
425℃
8.7GPa 25℃
R(110)
α(111)
R(101)
pressurizing at 565℃
heating at 8.7GPa
INTENSITY(arb.unit)
25.0
30.0
35.0
2θ Cu(Kα)
(converted from energy)

Fig.2–8

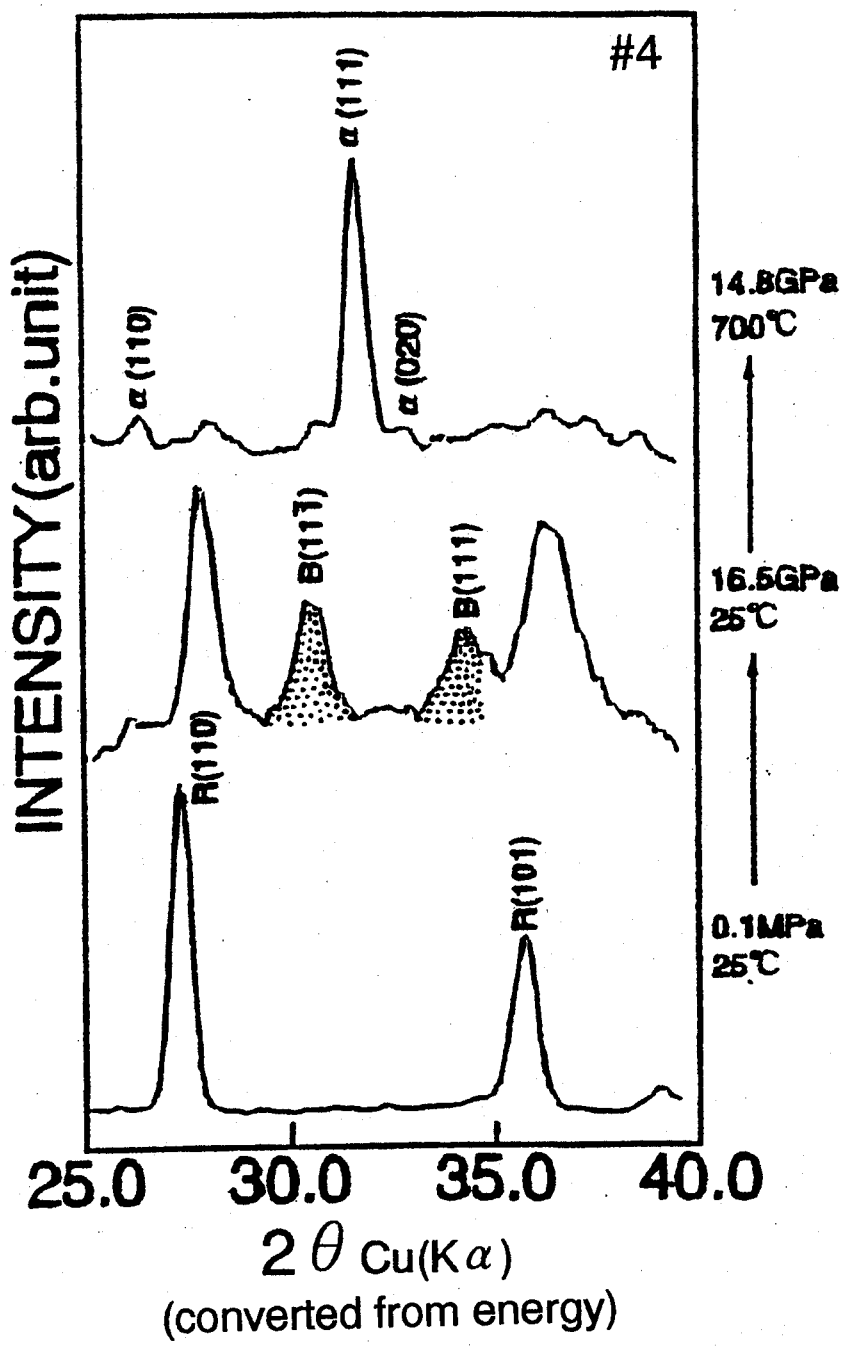
#4
α (111)
α (110)
α (020)
B(111)
B(111)
R(110)
R(101)
14.8GPa
700℃
16.5GPa
25℃
0.1MPa
25℃
INTENSITY(arb.unit)
25.0
30.0
35.0
40.0
2θ Cu(Kα)
(converted from energy)

Fig.2-9

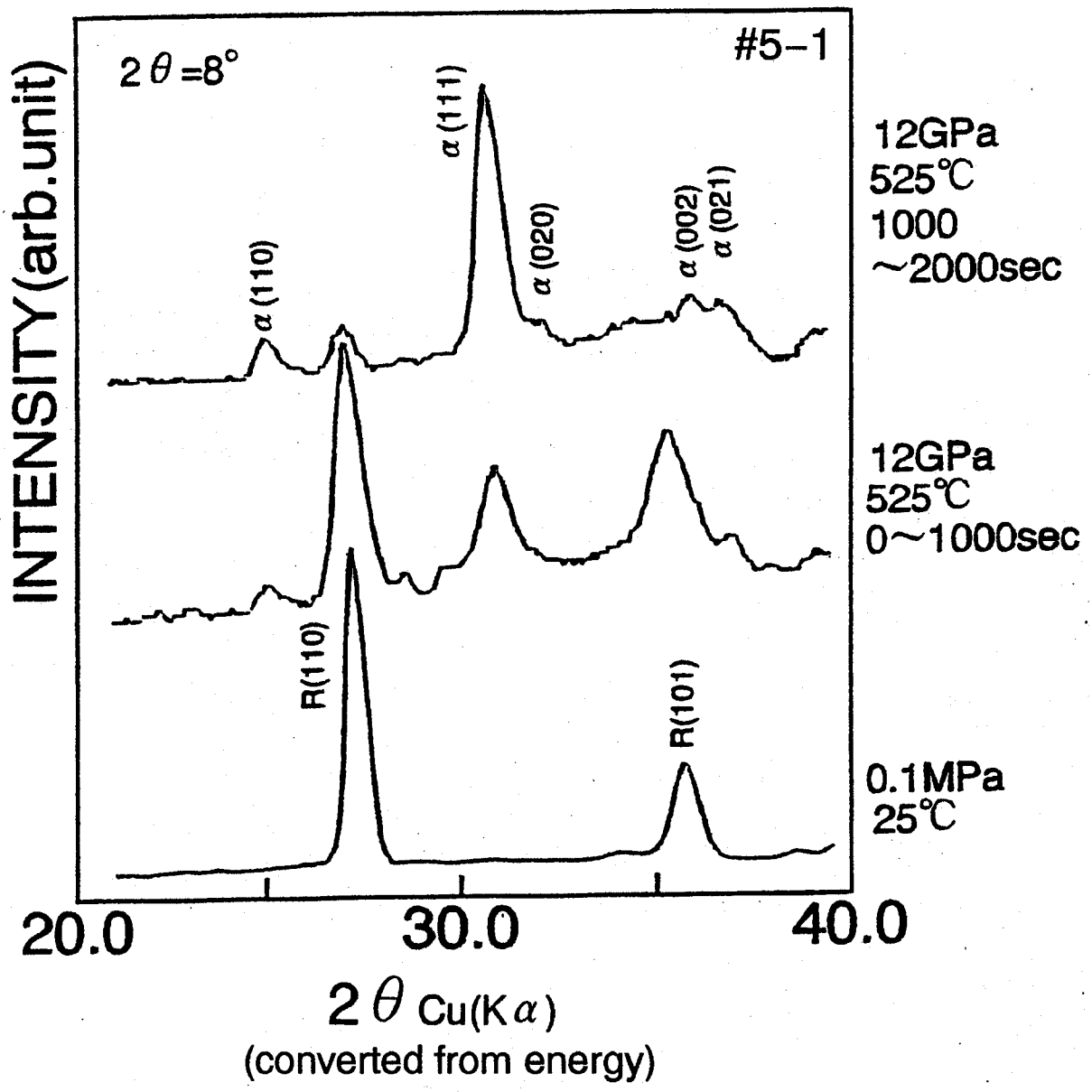
2θ=8°
#5-1
INTENSITY(arb.unit)
α(111)
α(110)
α(020)
α(002)
α(021)
12GPa
525℃
1000
~2000sec
12GPa
525℃
0~1000sec
R(110)
R(101)
0.1MPa
25℃
20.0
30.0
40.0
2θ Cu(Kα)
(converted from energy)

Fig.2-10

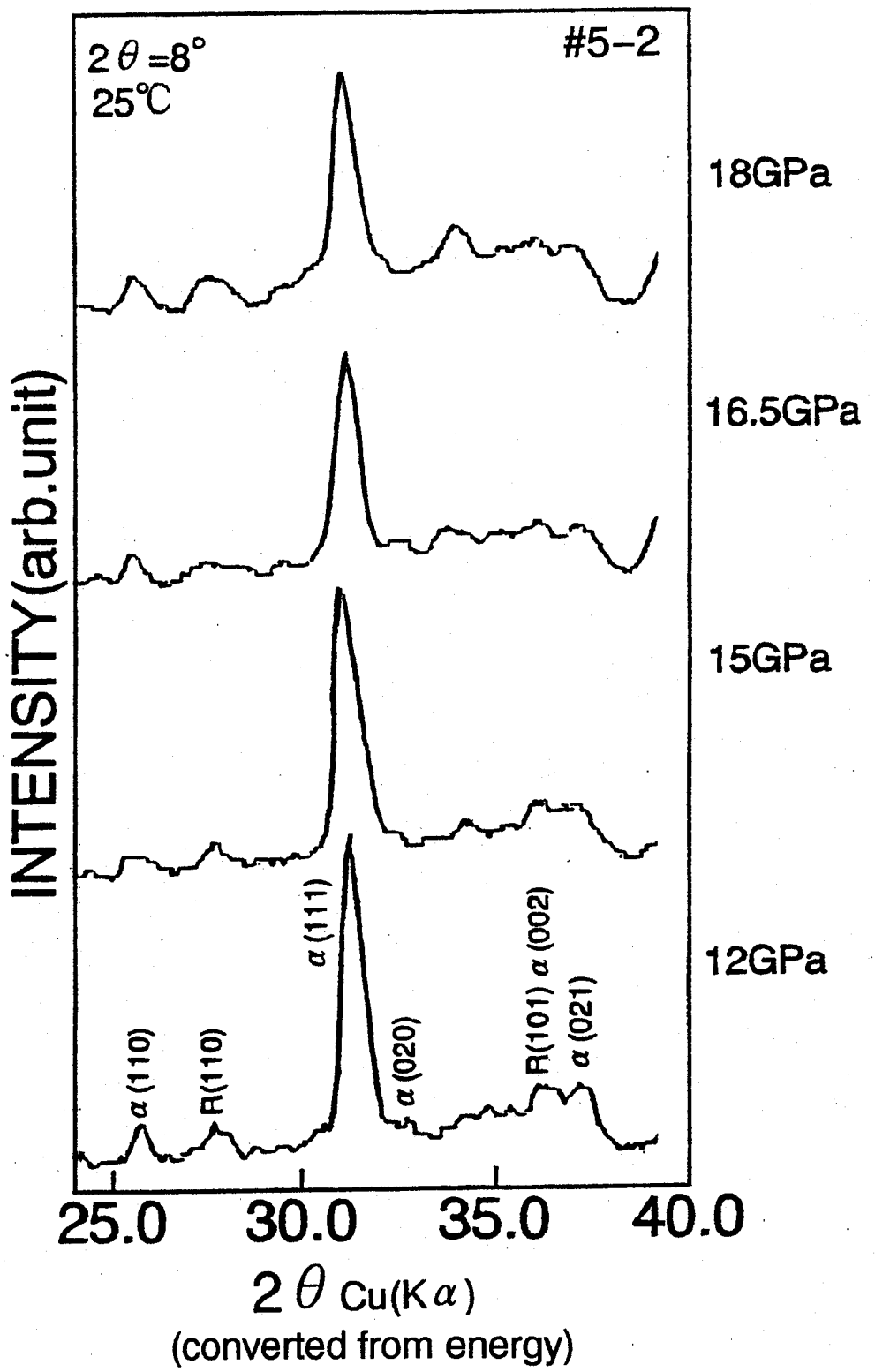
2θ=8°
25℃
#5-2
18GPa
16.5GPa
15GPa
12GPa
INTENSITY(arb.unit)
α (110)
R(110)
α (111)
α (020)
R(101) α (002)
α (021)
25.0
30.0
35.0
40.0
2θ Cu(Kα)
(converted from energy)

Fig.2-11

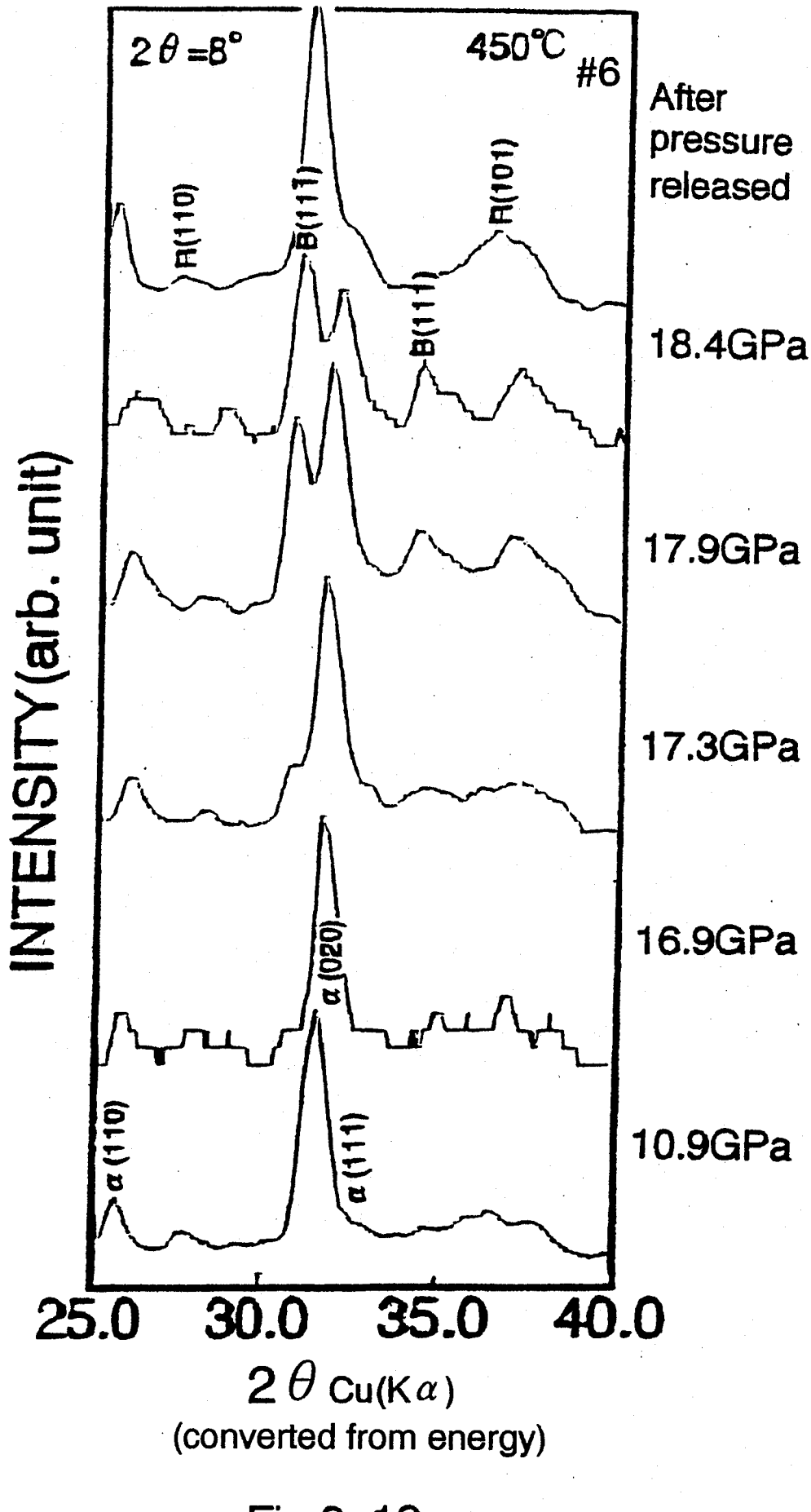
2θ =8°
450℃
#6
After pressure released
R(110)
B(111)
R(101)
B(111)
18.4GPa
17.9GPa
17.3GPa
16.9GPa
α (020)
α (110)
α (111)
10.9GPa
INTENSITY(arb. unit)
25.0
30.0
35.0
40.0
2θ Cu(Kα)
(converted from energy)

Fig.2-12

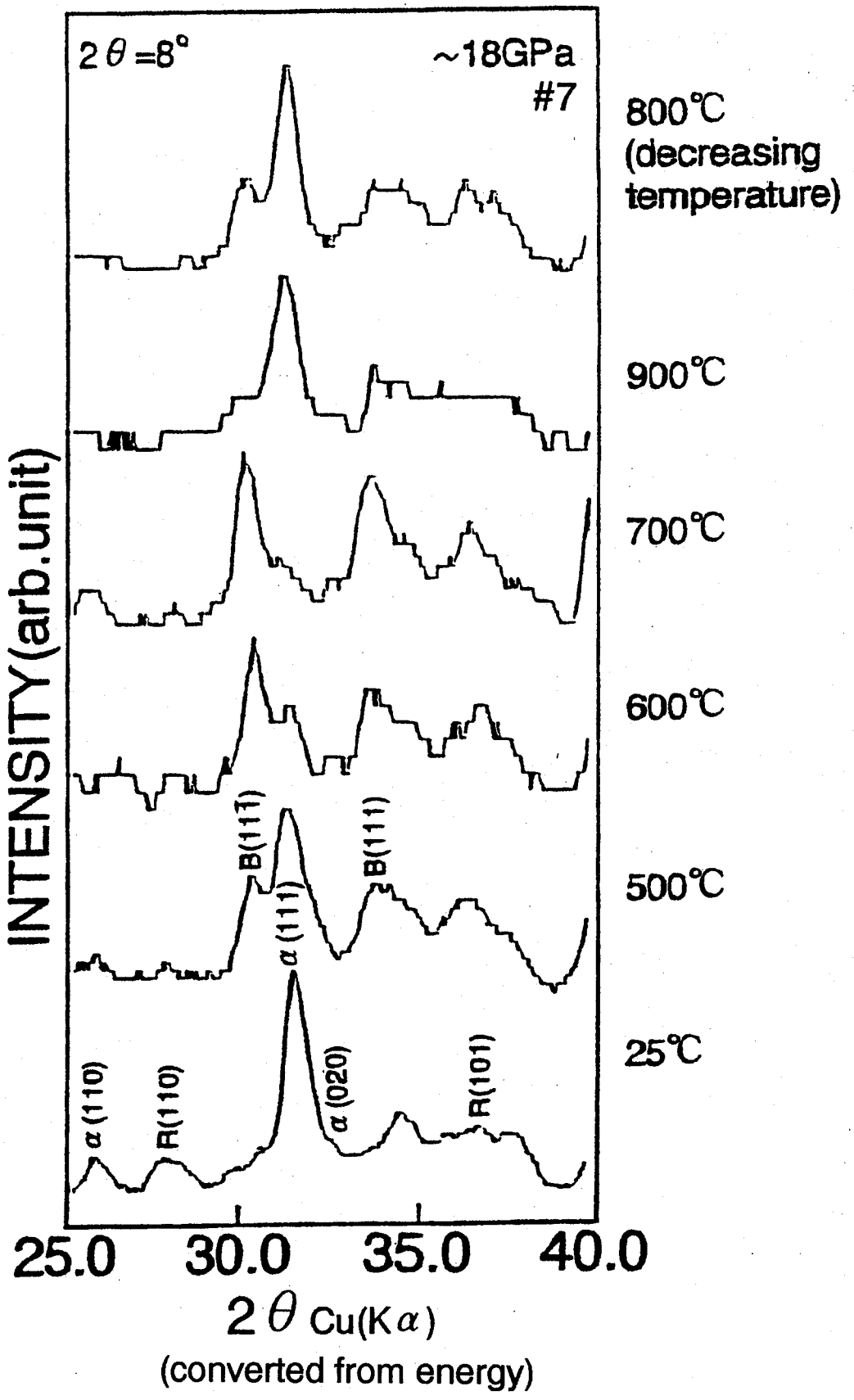
2θ =8°
~18GPa
#7
800℃
(decreasing
temperature)
900℃
700℃
600℃
500℃
25℃
INTENSITY(arb.unit)
B(11$\bar{1}$)
α(111)
B(111)
α(110)
R(110)
α(020)
R(101)
25.0
30.0
35.0
40.0
2θ Cu(Kα)
(converted from energy)

Fig.2–13

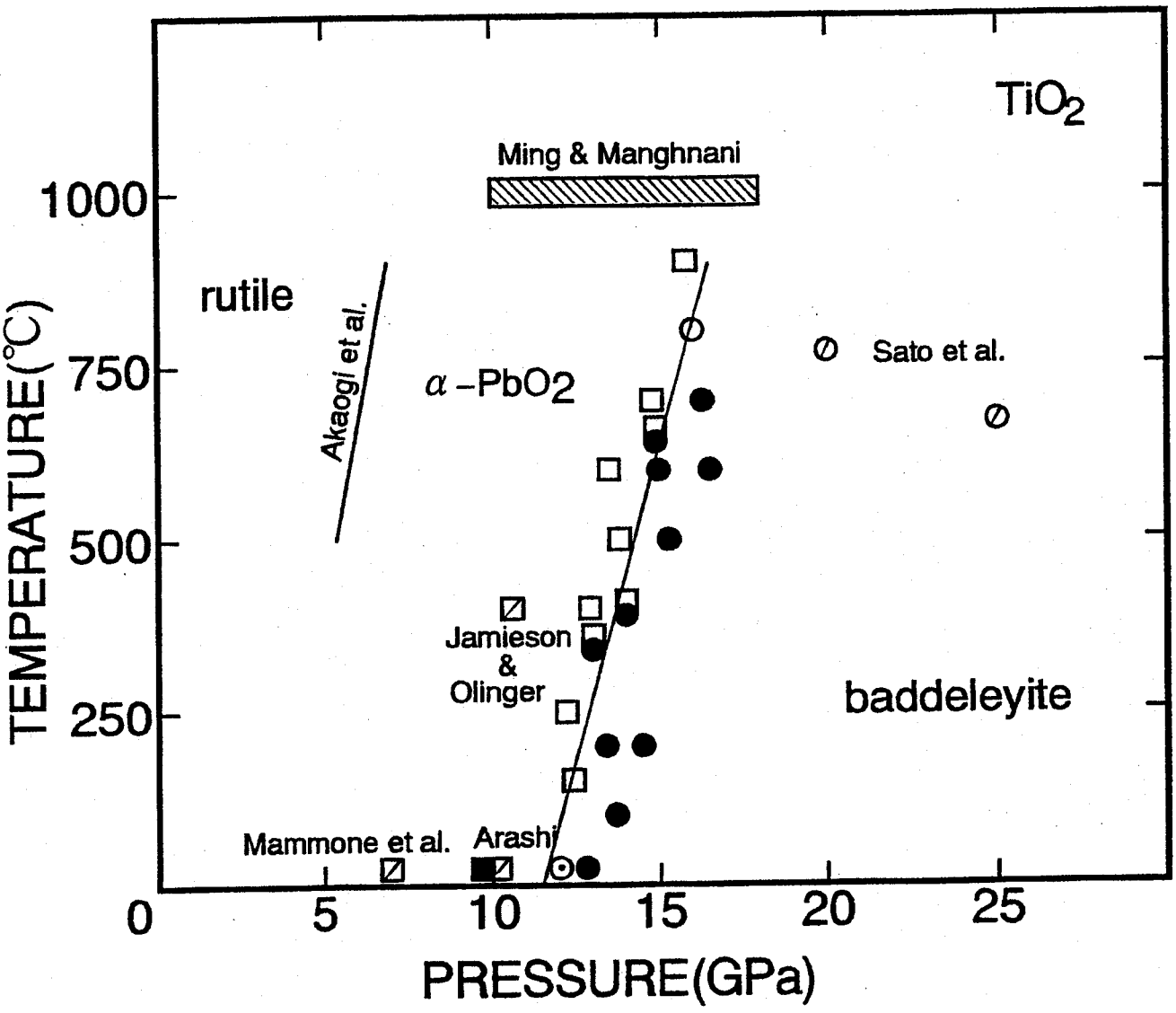

⊙:baddeleyite (from rutile by compression at RT).
■:α-PbO_2 (from baddeleyite by decompression at RT).
●→□:baddeleyite→α-PbO_2 (on heating).
□→○:α-PbO_2→baddeleyite (on cooling).

Fig.2-14

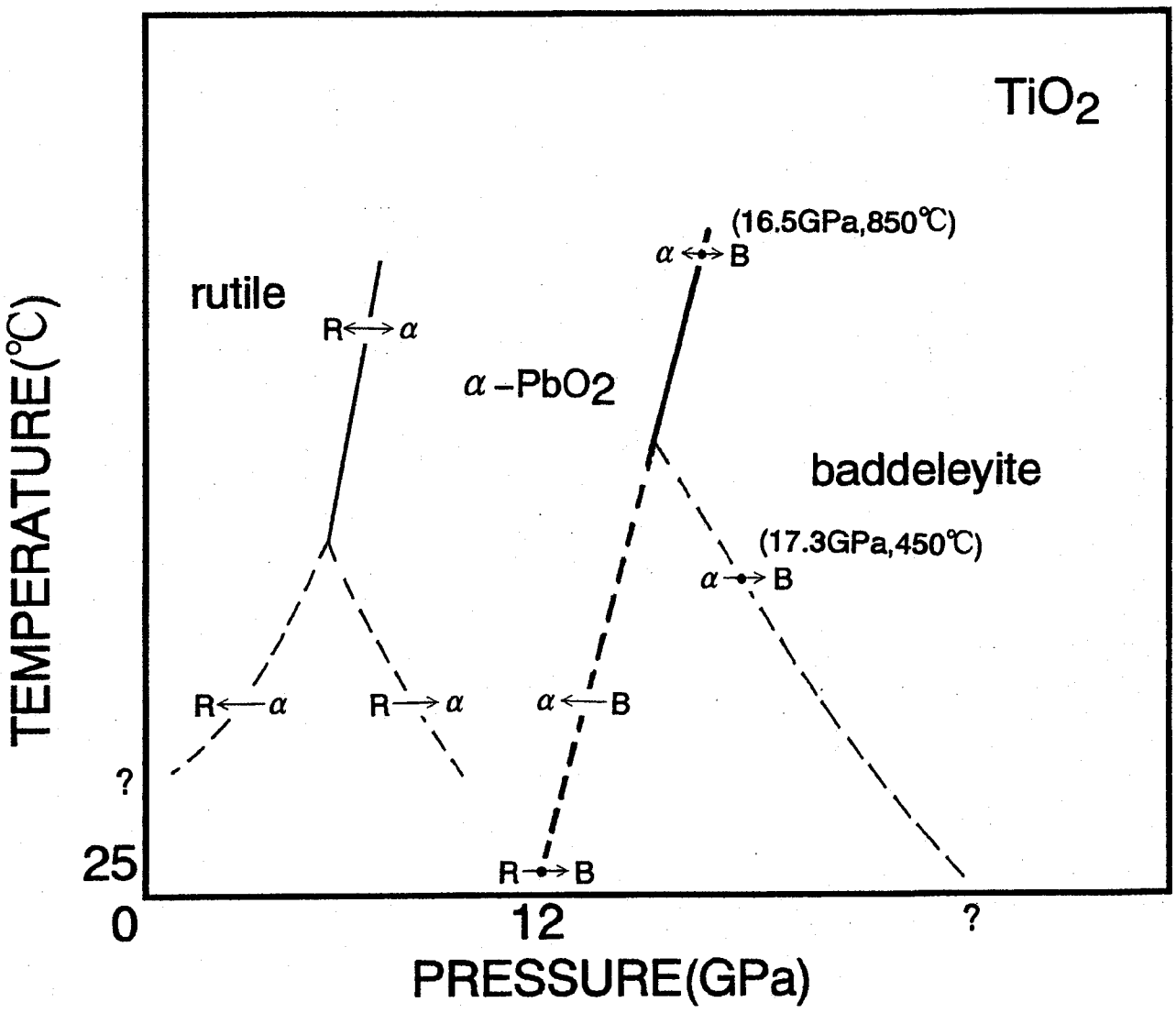
TiO2
(16.5GPa,850℃)
α↔B
rutile
R↔α
α-PbO2
baddeleyite
(17.3GPa,450℃)
α↔B
R←α
R→α
α←B
R↔B
TEMPERATURE(℃)
?
25
0
12
?
PRESSURE(GPa)

Fig.2-15

Chapter 3 Phase Transitions in HfO_2 at High Pressure and High Temperature

§1 Introduction

Three elements, Ti, Zr and Hf, belong to the same IVa group in the periodic table. Titanium dioxide, TiO_2, has been extensively studied under high pressure and high temperature as described in Chapter 2. The investigation of the pressure-induced transition in zirconium dioxide, ZrO_2, has been also carried out in the sense that ZrO_2 is one of the major components in the modern ceramics. On the contrary, hafnium dioxide, HfO_2, has been relatively less studied hitherto, although it behaves in the almost same manner as ZrO_2.

Baddeleyite, the stable phase of ZrO_2 at ambient conditions, has the monoclinic structure ($P2_1/c$, Z=4), in which a zirconium atom is coordinated irregularly with seven oxygen atoms. In addition, two other phases exist stably at atmospheric pressure; a tetragonal phase stable between 1170°C and 2370°C, and a cubic phase above 2370°C. Both of them are unquenchable to room temperature. On the other hand, two phases different from the above mentioned three phases are reported to exist at high pressures at room temperature[4,5]; they are called "orthorhombic I" (abbreviated as "ortho I" in the present paper) and "orthorhombic II" ("ortho II"), respectively. The lower pressure phase, ortho I, appearing at ~3.5 GPa, was once considered to have the space group of Pbcm (Z=4) by Kudoh[24] and Suyama[25], but a recent high resolution neutron powder diffraction study by Ohtaka et al.[26]

using the sample quenched to ambient conditions has revealed that it has the symmetry of Pbca, (Z=8). Ortho I seems to transforme to ortho II at pressure above 16.6 GPa and ortho II has the cotunnite ($PbCl_2$) structure (Pmnb, Z=4)[5], in which a zirconium atom is coordinated with nine oxygen atoms. The phase boundary between ortho I and ortho II of ZrO_2 were determined by Ohtaka et al.[25]. Very recently, a further transition to another high pressure phase (ZrO_2 IV) has been reported by Arashi et al.[28]. ZrO_2 IV seems to have a tetragonal symmetry at present.

On the contrary, there have been not so many studies about HfO_2 as those about ZrO_2 under pressure, but some of them suggest that the phase diagram of HfO_2 shows strong resemblance to that of ZrO_2. After Bendelini's first discovery[4] of the orthorhombic high pressure phase of HfO_2, Bocquillon et al.[29] confirmed its existence at pressure just below 2 GPa by the quench experiment. Very recently Ohtaka et al.[30] made a Rietveld refinement for X-ray and neutron diffraction and got the conclusion that it has the orthorhombic structure of Pbca, (Z=8), which is just the same as the ortho I of ZrO_2. Therefore, this orthorhombic phase is abbreviated as "ortho I" of HfO_2. The phase boundary between the monoclinic baddeleyite-type and the ortho I phase of HfO_2 determined by 3~6 GPa and 400~1100°C is also shown in Fig. 3-1. The tetragonal phase of both the dioxides exists in the higher temperature region.

Liu[5] made an X-ray diffraction experiment with the sample quenched from 16 GPa and about 1000°C and determined that the higher pressure phase of HfO_2 has an orthorhombic cotunnite ($PbCl_2$) type structure (abbreviated as "ortho II", too). There-

fore, ZrO_2 and HfO_2 have just the same sequence of structural transitions with increasing pressure: monoclinic (baddeleyiyte-type, $P2_1/c$) - orthorhombic I (Pmca) - orthorhombic II (cotunnite-type, Pmnb). However, these transitions do not take place so rapidly at room temperature. Especially, the ortho I-ortho II transition seems to be too sluggish to observe by X-ray diffraction. Adams et al.[31] studied HfO_2 up to 20 GPa at room temperature using synchrotron radiation and described that the initial monoclinic phase is still identified together with orhto I even at 20 GPa at room temperature and that high temperature experiments are indispensable to confirm the ortho II phase. In the present study, high-pressure and high-temperature X-ray diffraction experiments have been carried out to clarify the stable fields of ortho I and ortho II of HfO_2, which results in the determination of the *P*-T diagram.

§2 Experimental procedure

The starting material was a fine powder of HfO_2 having a grain size of ~100 nm and a purity of 98% with about 2% of ZrO_2. X-ray analysis showed that it consisted of the single phase of the monoclinic baddeleyite-type structure with the lattice parameters of a=5.112Å, b=5.172Å, c=2.257Å and β=98.7°. Since Hf is a heavy element with a large absorption coefficient of X-ray, the mixture of HfO_2 and amorphous boron with a proper ratio was used as the sample for the present high-pressure X-ray diffraction experiments.

In situ X-ray diffraction experiments, the details of which are the same as those for TiO_2 mentioned in Chapter 2, were carried out in the pressure range between 12~21 GPa at elevated temperatures up to 800°C. Usually the pressure was increased at room temperature, and then, the temperature was increased under the constant oil-pressure of the press. Typical X-ray exposure time was 1000~3000 sec under high pressure and high temperature conditions.

In addition, the precise X-ray analyses using a microdiffractometer with CuKα radiation and a PSPC detector were performed for the sample recovered from the final pressure-temperature conditions of each run. As the ortho I and ortho II of HfO_2 can be quenched to ambient conditions, this analysis proved to be very useful; the patterns of the three phases of HfO_2 are very difficult especialiy to identify in the case where these phases coexist.

§3 On X-ray diffraction patterns of HfO_2

The d-values of the monoclinic, ortho I and ortho II phases of HfO_2 at ambient conditions are listed in Table 2 and shown in Fig. 3-2: the data of the monoclinic phase was obtained by Adam and Rogers[32](JCPDS #6-0318), the ortho I by Bocquillon[29] and ortho II by Liu[5]. The real patterns obtained by microdiffractometer in the present study are also presented in Fig. 3-3: the pattern of the monoclinic phase is of the starting material, and those of ortho I and ortho II are of the samples quenched from (I) 12 GPa and 700°C, and (II) 21 GPa and 450°C, respectively.

The three phases have relatively complex patterns with many diffraction lines. Taking into consideration that their strong reflections concentrate in almost the same range of d=2.5~3.1Å (2θCuKα=36°~29°), SSD was set at 2θ=8° in the energy dispersive geometry of the present system. When the monoclinic phase transforms to ortho I, two lines of the monoclinic phase, M($11\bar{1}$) and M(111), disappear and instead a new line of ortho I, I(111), appears at the position between the disappearing two lines. By a further transition from ortho I to ortho II, I(111) disappears and new two lines of ortho II, II(011) and doublet II(102+200), appear. But the d-value of II(011) is very close to that of I(111), and the doublet II(102+200) close to M(111). Therefore, the distinction between the two high pressure phases becomes very difficult in the case where the initial monoclinic phase remains in coexistence with them. The gradual changes of pressure and temperature were adopted in each run for the systemtic phase identification.

§4 Results

The lattice parameters, the unit cell volume and the volume per molecule of the three phases of HfO_2 obtained at ambient conditions are listed in Table 3, together with the values by previous investigators. The volume decreases of about 3.8% and 11.5% are recognized for the monoclinic → ortho I and the ortho I → ortho II transition, respectively.

Two examples of the change of the X-ray diffraction patterns

of HfO_2 with increasing pressure and then temperature are shown in Figs. 3-4 and 3-5. As shown in Fig. 3-4, when the monoclinic phase was compressed at room temperature, the diffraction line 111 of the ortho I, that is I(111), appeared at 9 GPa and became clearer at 12 GPa. Then, I(111) grew up gradually with increasing temperature. The pattern of 12 GPa and 500°C indicates that the monoclinic phase disappeared and the single phase of ortho I was formed. I(020) and I(002,200) are also clearly observed at these conditions. The pattern for the sample recovered from 12 GPa and 700°C (Fig. 3-3(b)) is completely of the single phase of ortho I. All the *P-T* conditions where the patterns of Fig. 3-4 except that at 0.1 MPa and 25°C were obtained belong to the stable region of ortho I.

Figure 3-5 shows the patterns at ~16 GPa. To identify whether the phase appearing at high pressure is ortho I or ortho II, X-ray patterns were obtained at temperatures higher than 500°C, at which the monoclinic phase disappeared at ~12 GPa as shown in Fig. 3-4. The pattern obtained at ~16 GPa and 600°C represents the almost single phase of ortho II. With increasing temperature, the intensity of II(102,200) became stronger as expected for ortho II, although the reason is not clear. The sample recovered from 16 GPa and 700°C had the pattern of ortho II.

Such *in situ* X-ray diffraction experiments were performed along the other paths and the careful identification of the phases was made by the microdiffractometer for the sample recovered from various final pressures and temperatures.

§5 Discussion

5.1 Phase boundary between ortho I and ortho II of HfO_2

Combining the results by *in situ* X-ray diffraction at high pressure and high temperature with those by the microdiffractometer for the quenched samples, the regions where the ortho I and ortho II phases are formed are indicated in Fig. 3-6. The pressure values on the abscissa are corrected for high temperature according to the method described in Chapter 1. In Fig. 3-6 the data point identified by the microdiffractometer after the *in situ* X-ray diffraction are marked by closed symbols. The phase boundary between the ortho I and ortho II is located at about 14 GPa, however, the slope of the boundary is too sharp to determine in the present study whether it is positive or negative.

The region where the ortho II phase was confirmed by Liu[5] with the quenched samples is plotted too in Fig. 3-6. His result is agreement with the present results. On the contrary, the result by Adams et al.[31] indicating that the sample at 20 GPa and room temperature were a mixture of the monoclinic and ortho I phases seems to be against the present boundary. This may result from the sluggishness of the ortho I-ortho II transition. Figures 3-7(a) and (b) are X-ray patterns obtained in the present study. The gradual formation of ortho I phase with increasing pressure and then temperature is observed in Fig. 3-7(a), which is the process almost similar to that in Fig. 3-4. On the other hand, Fig. 3-7(b) represents the formation of the ortho II phase at 18 GPa and 700°C, which is similar to that in Fig. 3-5. The phase

identification of the pattern at 18 GPa and 25°C is difficult. Comparing the pattern at 12 GPa and 25°C in Fig. 3-7(a) with that at 18 GPa and 25°C in Fig. 3-7(b), the amount of the residual monoclinic phase at 18 GPa is less than that at 12 GPa. Neverthless, the peak corresponding to M(111) is still large. Therefore, M(111) is assumed to be the addition of M(111) and II(102,200). Then, the left side of it is considered to be not I(111), but II(011). Therefore, the ortho II phase appeared at 18 GPa and room temperature in the present study.

Adams et al.[31] suggested the possibility that the phase transition from the monoclinic to, perhaps, ortho II phases may begin near 10 GPa at room temperature based on the relative intensities of M($11\bar{1}$) and M(111) and the change of the length of the a-axis of the monoclinic phase. However, the patterns obtained in the present study (Fig. 3-4) does not support their suggestion about the phase transition to ortho II near 10 GPa.

5.2 On the monoclinic–ortho I phase transition

As shown in Figs. 3-4 and 3-7(a), the transition from the parent monoclinic phase to the ortho I phase occurred when pressure was applied, and the amount of the formed ortho I phase was dependent on the applied pressure and temperature; for example, the two phases coexisted under 15 GPa and 200°C (sample A) in Fig. 3-7(a) and the single phase of ortho I was formed under 12 GPa and 700°C (sample B) in Fig. 3-4. However, as shown from the comparison of these two figures , the reverse transition from the ortho I to the monoclinic phase, which occurred by decreasing the

temperature and releasing the pressure to ambient conditions, was quite different between sample A and B. That is, the reverse transition occured in the sample A, but did not in the sample B. The reason of such difference has not been clarified yet in the present study, but may be due to the difference in coexistence of the monoclinic phase and the ortho I phase formed martensitically, considering that other physical situations seem to be the same between samples A and B. In other words, it may be due to how much the elastic strain caused by the coexistence of the two phases and the plastic strain caused by the accommodation of the volume change associated with the transition are introduced in the sample, taking account of the fact that both strains are well known to influence the reverse transition: the elastic strain promotes and the plastic strain depresses the reverse transition. Because of the above reason, we can qualitatively say that the reverse transition occurs in the sample A, but not in the sample B although quantitative analysis for those strains on the reverse transition must be needed.

5.3 Phase diagrams of HfO_2 and ZrO_2

In Fig. 3-6 is also shown the phase boundaries among the monoclinic, ortho I and tetragonal phases determined by Ohtaka et al.[30]; the boundary between the monoclinic and ortho I phases were based on the observation from the monoclinic to ortho I phase transition.

On the other hand, the phase diagram of ZrO_2 is shown in Fig. 3-8, in which the boundary between the monoclinic and ortho

I phases and that between the ortho I and ortho II phases were determined by Block et al.[33] and Ohtaka et al.[27], respectively, using the monoclinic phase as the starting phase. There is a fair resemblance as to the transition pressures in the phase diagrams of HfO_2 (Fig. 3-6) and ZrO_2 (Fig. 3-8). Probably, this resemblance results from the fact that the two elements, Zr and Hf, have almost identical sizes: Adams et al.[31] described that "the Hf atom is affected by the lanthanide contraction which, despite the larger number of electron shells, reduces its size almost to that of Zr".

The boundary determined in the present study was based on the observation of the transition from the monoclinic to ortho II phase. For determining the thermal equilibrium boundary, a direct observation of ortho I ↔ ortho II phase transition is necessary. Such studies are planned in our laboratory.

§6 Conclusion

The present study on the phase transitions in HfO_2 at high pressure and high temperature gives the following results:

(1)The *P-T* regions where the ortho I and ortho II phases were formed from the baddeleyite phase were determined. The formation boundary between the ortho I and ortho II phases lies around 14 GPa in the temperature range between 400°C and 700°C.

(2)The phase diagram of HfO_2 resembles as to that of ZrO_2.

(3)At room temperature the monoclinic → ortho II phase transition was sluggish and accomplishd at 18 GPa which is higher than the pressure extrapolated from the transition at high tem-

perature.

(5)A direct observation of ortho I ↔ ortho II phases is necessary to determined the equilibrium boundary between the ortho I and ortho II phases.

Table 3–1 X-ray diffraction data of the three phases of HfO_2 at ambient conditions

monoclinic		Ortho I		Ortho II	
(hkl)	d (Å)	(hkl)	d (Å)	(hkl)	d (Å)
100	5.07				
011	3.68				
110	3.61				
$11\bar{1}$	3.15			002	3.24
				101	2.950
111	2.82	111	2.945		
		020	2.618	012	2.790
				111	2.603
002 . 020	2.59	002	2.545		
200	2.52	200	2.519		
102	2.48	021	2.324		
012, 021, 120	2.32				
$21\bar{1}$	2.196				
102 . $12\bar{1}$	2.171				
		211	2.069	112, 120	2.14
				121	2.025
112	2.006				
211 . 202	1.981				
212 . 022	1.838	022	1.819		
		220	1.809		
220	1.807			103	1.806
$12\bar{2}$	1.794				
		202	1.780		
$22\bar{1}$	1.768			113	1.714
		221	1.703		
300 . 202	1.684	212	1.683		
				200	1.653
221	1.653	130	1.646		
013, 031, $11\bar{3}$	1.634				
				032, 201	1.608
311, 310, 212	1.600	310	1.599		
$13\bar{1}$	1.580			131	1.566
		131	1.564		
131 . $30\bar{2}$	1.533	113	1.528		
		311	1.517		
				123	1.513
	1.501				
	1.486	222	1.470		
	1.467				
	1.439				
		023	1.417	212, 220	1.422
	1.410				
				024	1.394
		302	1.393		
		132	1.379		
		213	1.353		
	1.352				
	1.318	040	1.307		
	1.299				
	1.295	041	1.265		
	1.263				
	1.256	400	1.252		
	1.237				
		330	1.205		
		411	1.183		
		133	1.177		
				115	1.176
		331	1.172		
		313, 240	1.157		
		024	1.138		
				214	1.133
		204, 420	1.129		
				143	1.098
				310	1.084
				240	1.063
				044, 052	1.051
				151	1.038
				242, 135	1.010
				234	0.9802

Table 3–2 Crystallographic data of the three phases of HfO_2 at ambient conditions.

	monoclinic		ortho I		ortho II	
space group	$P2_1/c$		Pbca		Pmnb	
Z	4		8		4	
	JCPDS#6-0318	the present study	Ohtaka et al[24]	the present study	Liu[5]	the present study
a(A)	5.12	5.112(9)	10.0172(2)	10.008(10)	3.328(2)	3.32(2)
b(A)	5.18	5.172(17)	5.2276(1)	5.230(9)	5.565(4)	5.55(3)
c(A)	5.25	5.257(8)	5.0598(2)	5.048(10)	6.461(5)	6.46(4)
β°	98°	98.7° ± 0.1°				
V(A^3)/unit cell	137.9	137.3(5)	265.0	264.2(5)	119.7	119(1)
V(A^3)/molecule	34.5	34.5(5)	33.1	33.0(5)	29.9	29.7(1)

Figure Captions

Fig. 3-1 Phase boundaries among the monoclinic, ortho I and tetragonal phases of HfO_2 by Bocquillon et al.[27] and Ohtaka et al.[28].

Fig. 3-2 X-ray diffraction data of the three phases of HfO_2 at ambient conditions.

Fig. 3-3 X-ray diffraction patterns of the three phases of HfO_2 obtained at ambient conditions in the present study.

Fig. 3-4 X-ray diffraction patterns of HfO_2 indicating the transition from the monoclinic to ortho I phase in the increasing pressure and then increasing temperature processes. The formation of the single phase of ortho I is seen at 12 GPa and 500°C.

Fig. 3-5 X-ray diffraction patterns of HfO_2 indicating the transition from the monoclinic to ortho II phase by heating at ~16GPa.

Fig. 3-6 *P-T* phase diagram of HfO_2. The triangles and circles represent the formation of the ortho I and ortho II phase, respectively, from the monoclinic phase in the present study. The closed symbols mean that the phase was examined by a microdiffractometer after quenched to ambient conditions. The boundary between the ortho I and II phases lies at ~14GPa. The boundaries among the monoclinic, ortho I and tetragonal phases are by Ohtaka et al.[28]. The formation of the ortho II phase by Liu[5] and the ortho I phase by Adams et al.[29] are also

plotted.

Fig. 3-7 X-ray diffraction patterns of HfO_2 indicating the formation of (a)ortho I and (b)ortho II phase at high pressures and high temperatures.

Fig. 3-8 *P-T* phase diagram of ZrO_2 determined by Block et al.[31] and Ohtaka et al.[25] using the starting material of the monoclinic ZrO_2 (baddeleyite).

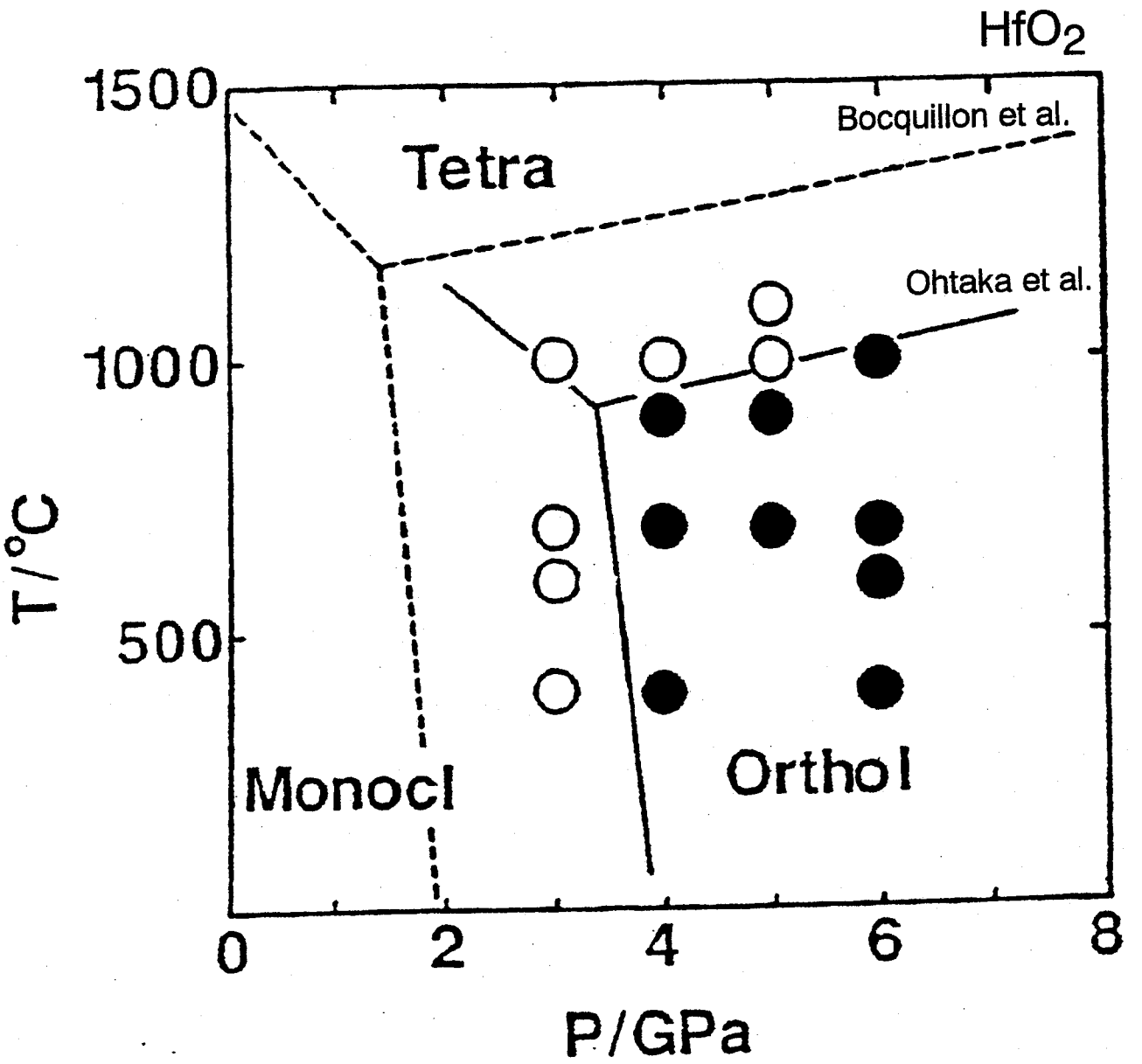
HfO2
1500
1000
500
T/°C
Bocquillon et al.
Ohtaka et al.
Tetra
Monocl
Orthol
0
2
4
6
8
P/GPa

Fig.3–1

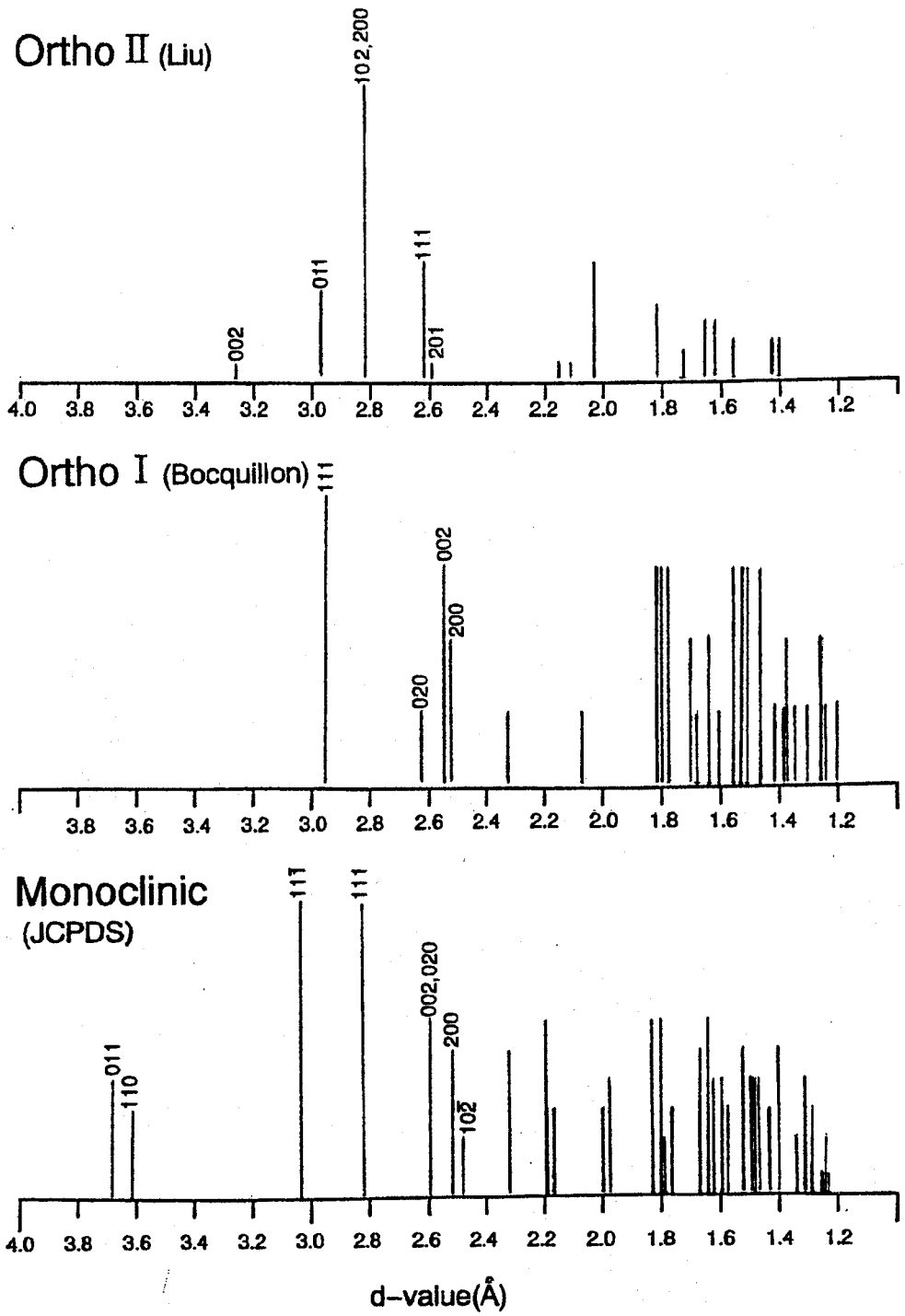
Ortho II (Liu)
002
011
102,200
111
201
4.0 3.8 3.6 3.4 3.2 3.0 2.8 2.6 2.4 2.2 2.0 1.8 1.6 1.4 1.2
Ortho I (Bocquillon)
111
020
002
200
3.8 3.6 3.4 3.2 3.0 2.8 2.6 2.4 2.2 2.0 1.8 1.6 1.4 1.2
Monoclinic
(JCPDS)
011
110
111
111
002,020
200
102
4.0 3.8 3.6 3.4 3.2 3.0 2.8 2.6 2.4 2.2 2.0 1.8 1.6 1.4 1.2
d-value(Å)

Fig.3-2

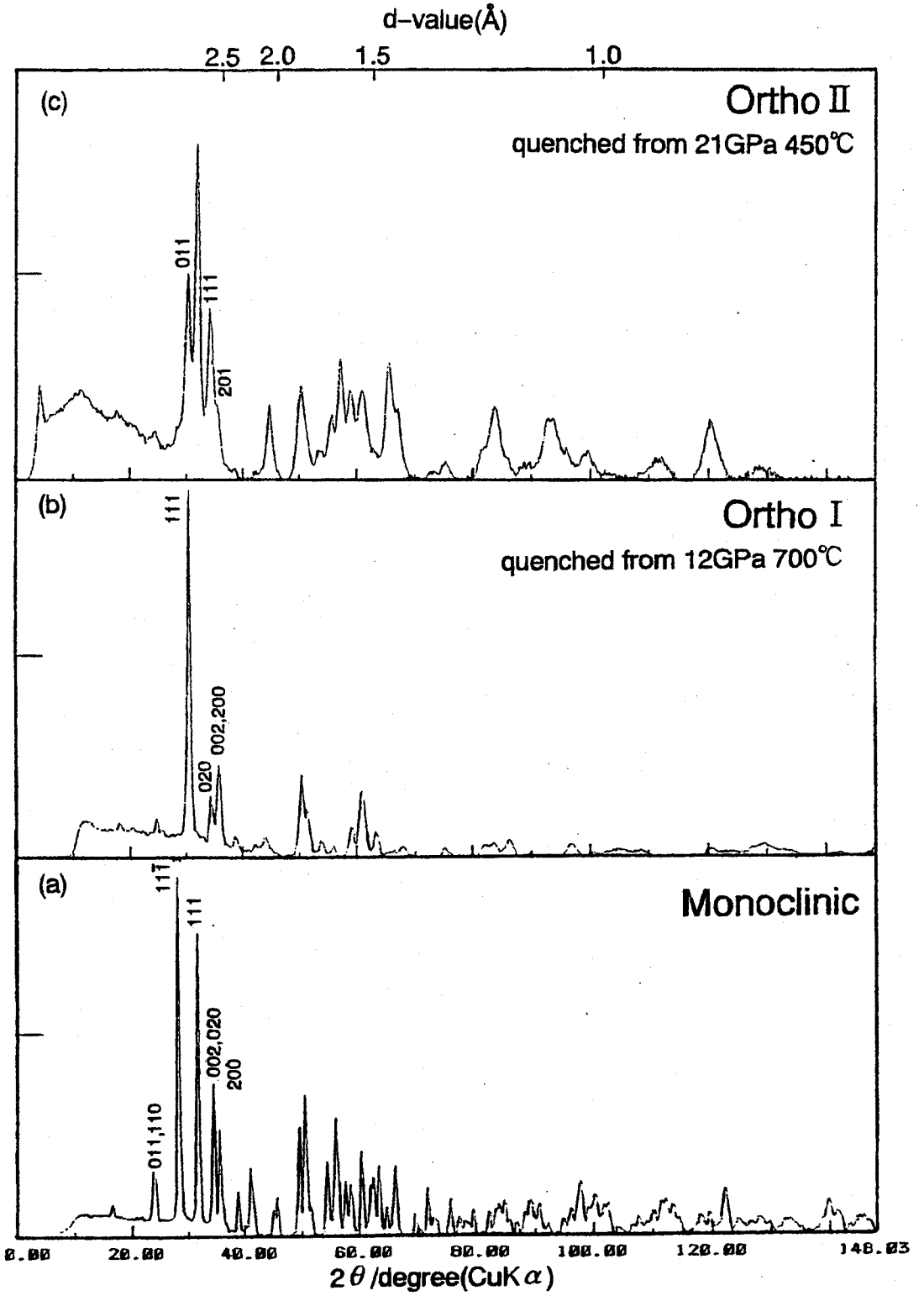
d-value(Å)
2.5
2.0
1.5
1.0
(c)
Ortho II
quenched from 21GPa 450℃
011
111
201
(b)
Ortho I
quenched from 12GPa 700℃
111
020
002,200
(a)
Monoclinic
111
111
011,110
002,020
200
0.00
20.00
40.00
60.00
80.00
100.00
120.00
140.03
2θ/degree(CuKα)

Fig.3-3

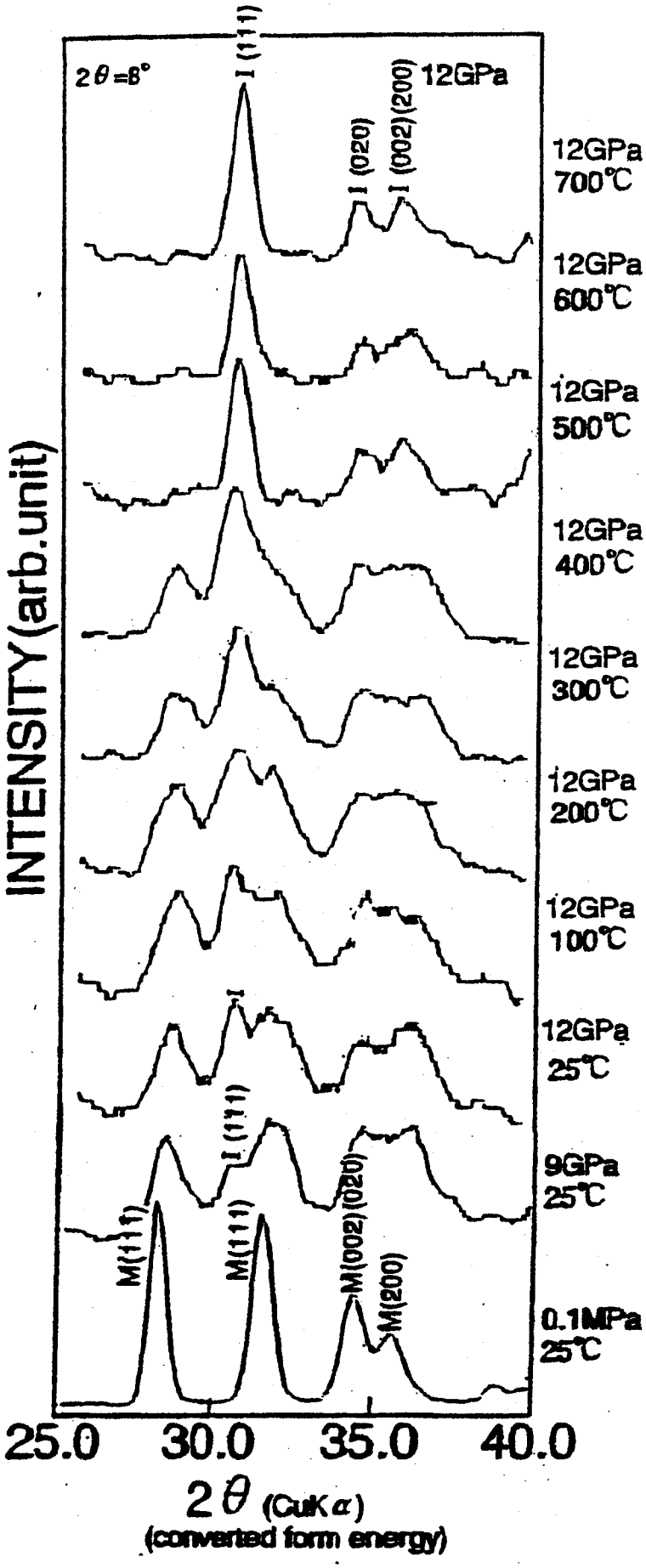
2θ=8°
I (111)
I (020)
I (002)(200)
12GPa
12GPa 700℃
12GPa 600℃
12GPa 500℃
12GPa 400℃
12GPa 300℃
12GPa 200℃
12GPa 100℃
12GPa 25℃
9GPa 25℃
0.1MPa 25℃
M(111)
M(111)
M(002)(020)
M(200)
INTENSITY(arb.unit)
25.0
30.0
35.0
40.0
2θ (CuKα)
(converted form energy)

Fig.3–4

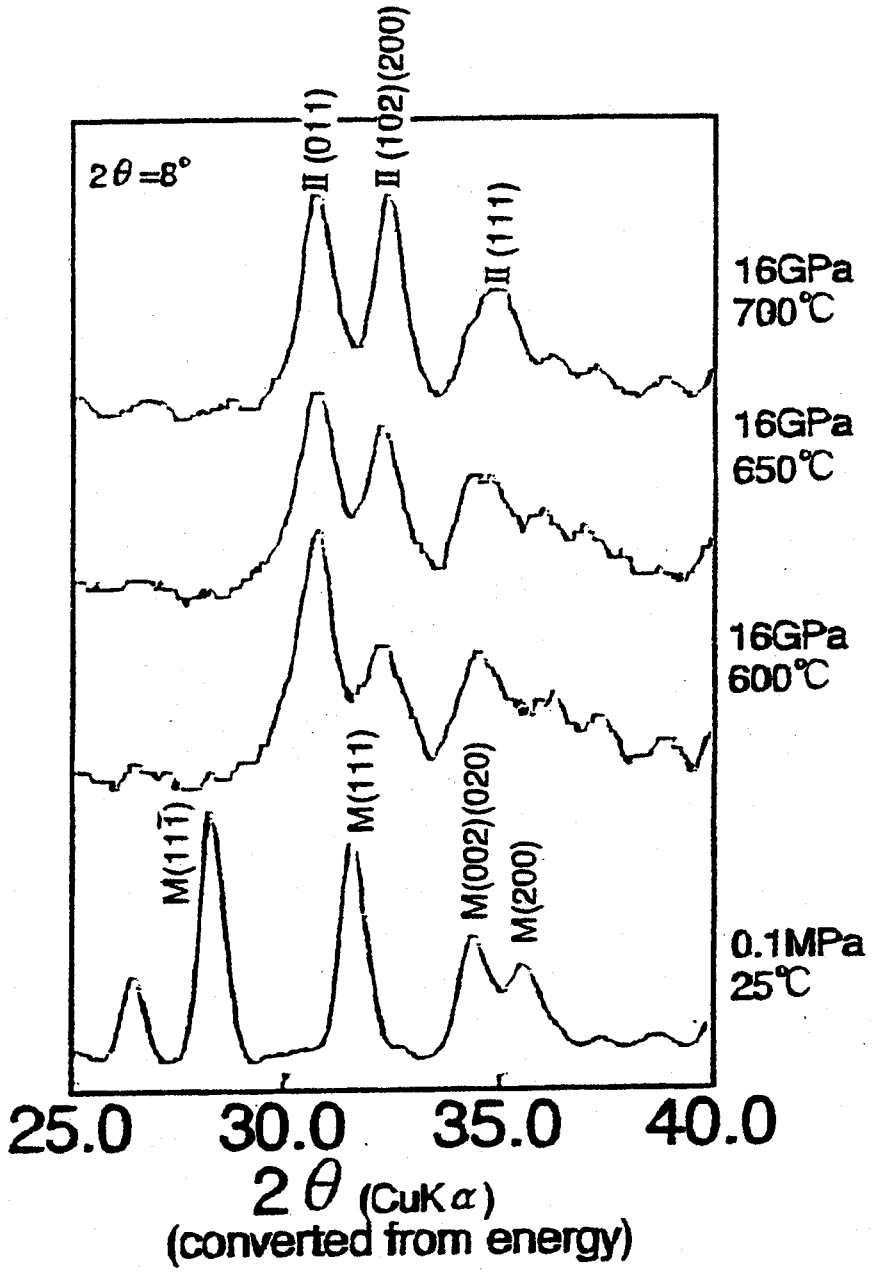
2θ=8°
II (011)
II (102)(200)
II (111)
16GPa
700℃
16GPa
650℃
16GPa
600℃
M(11$\bar{1}$)
M(111)
M(002)(020)
M(200)
0.1MPa
25℃
25.0
30.0
35.0
40.0
2θ (CuKα)
(converted from energy)

Fig.3-5

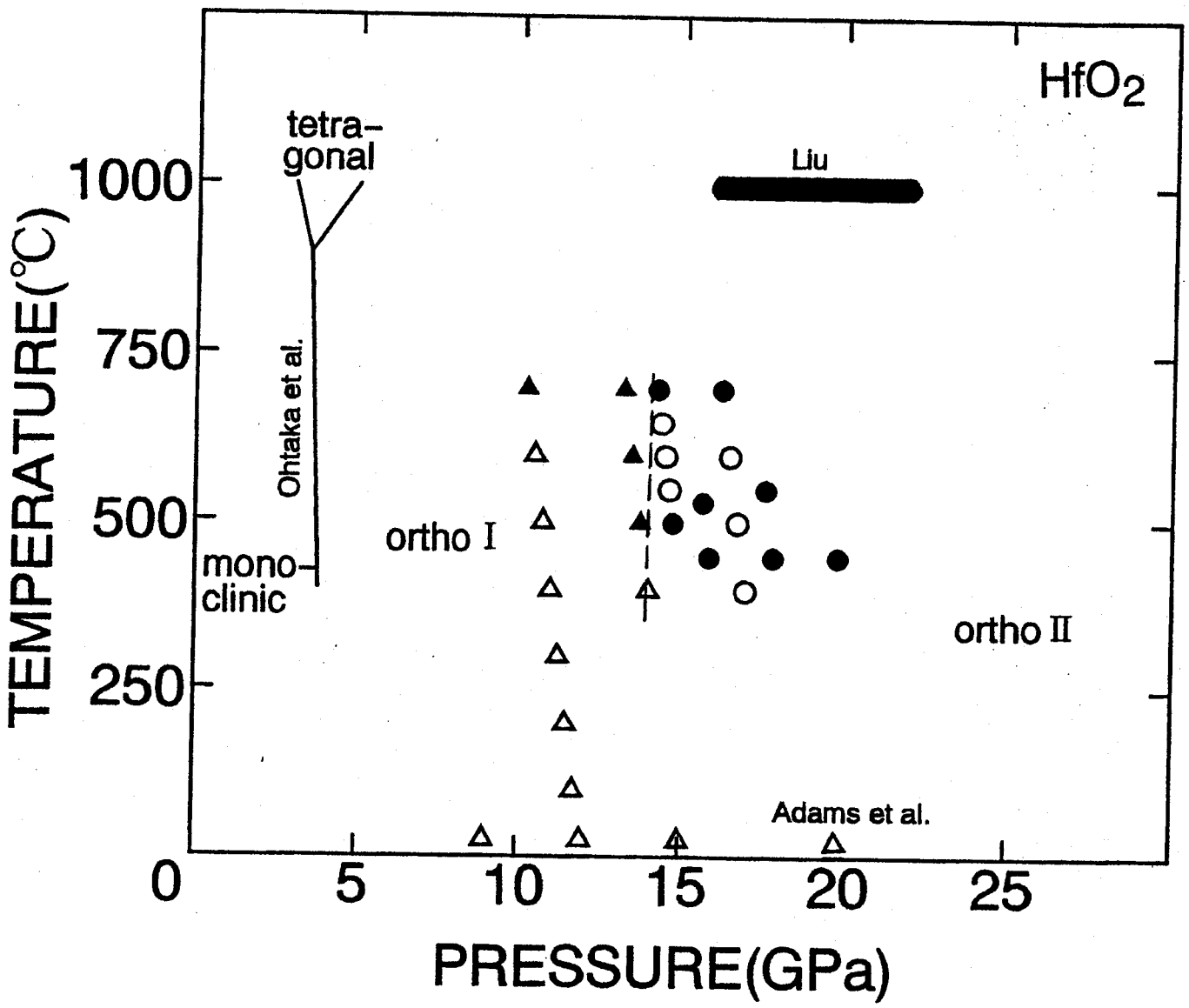
HfO2
tetra-
gonal
Liu
1000
750
500
250
0
TEMPERATURE(°C)
Ohtaka et al.
mono-
clinic
ortho I
ortho II
Adams et al.
5
10
15
20
25
PRESSURE(GPa)

Fig.3-6

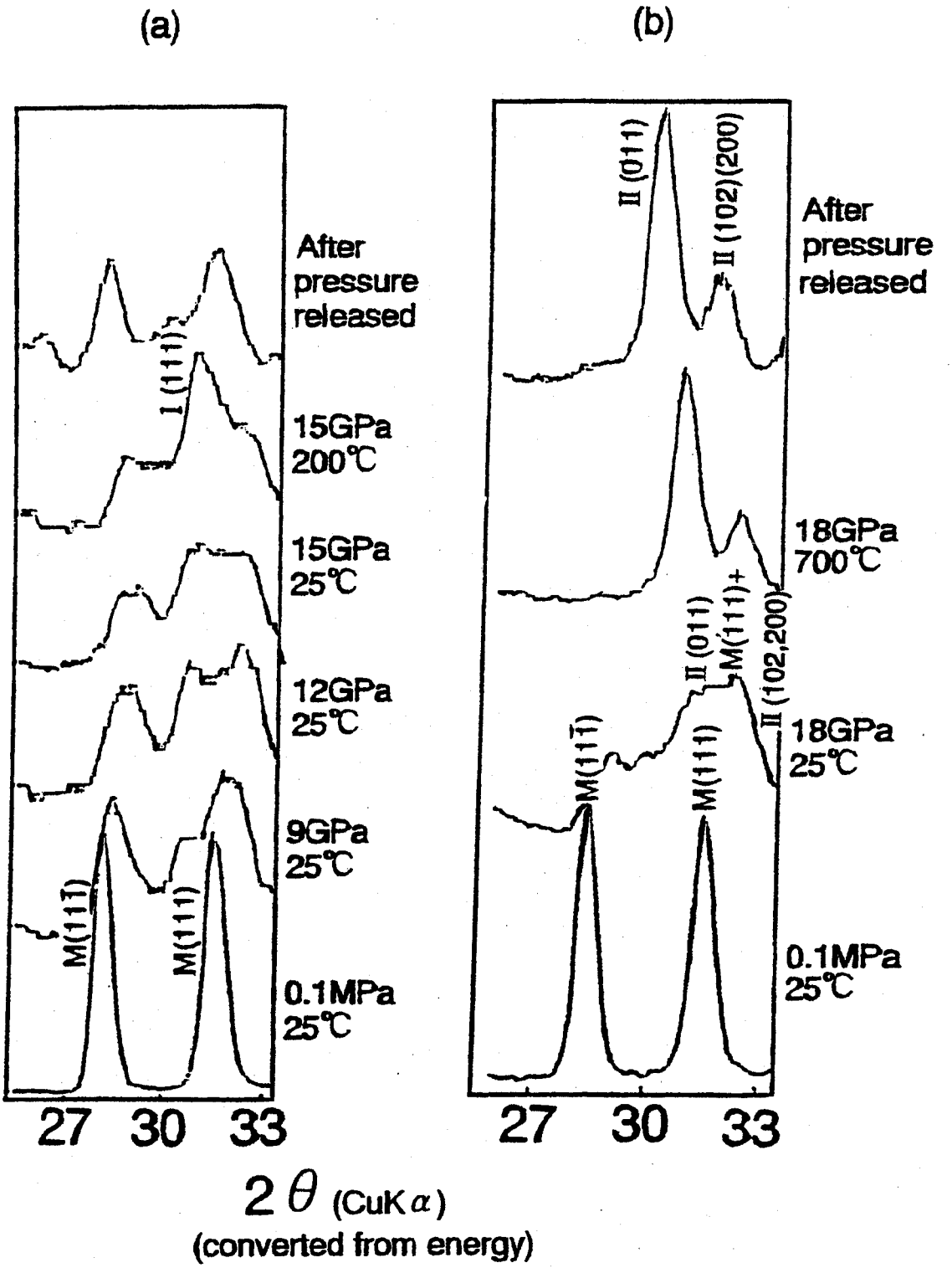
(a)
(b)
After pressure released
15GPa 200℃
15GPa 25℃
12GPa 25℃
9GPa 25℃
0.1MPa 25℃
I (111)
M(11$\bar{1}$)
M(111)
II (011)
II (102)(200)
18GPa 700℃
M(111)+
II (011)
II (102,200)
18GPa 25℃
M(11$\bar{1}$)
M(111)
0.1MPa 25℃
27 30 33
27 30 33
2θ (CuKα)
(converted from energy)

Fig.3–7

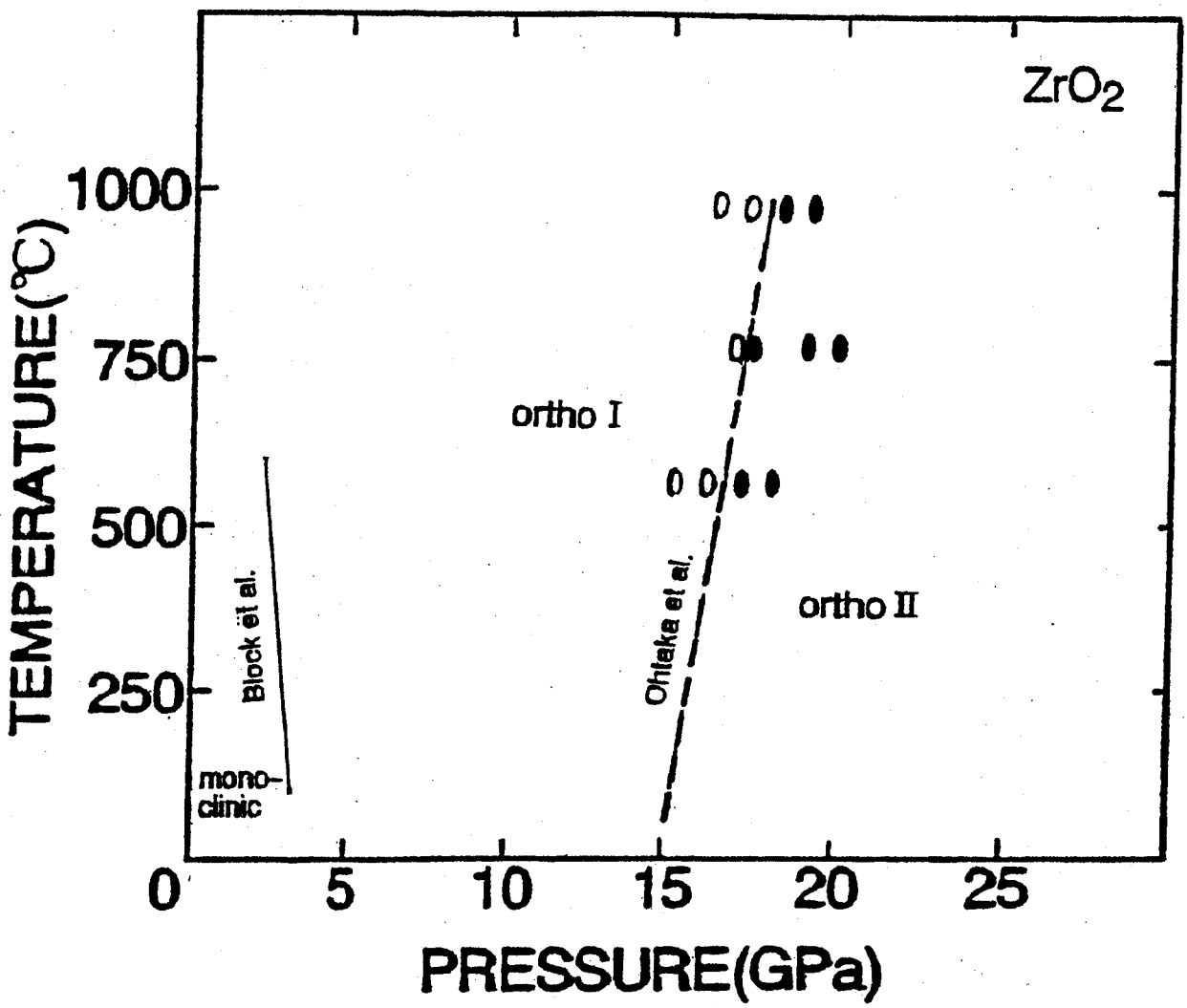
ZrO2
1000
750
500
250
0
TEMPERATURE(℃)
5
10
15
20
25
PRESSURE(GPa)
ortho I
ortho II
Block et al.
Ohtaka et al.
mono-
clinic

Fig.3-8

References

[1]R.G. McQueen, J.C. Jamieson, and S.P. Marsh, "Shock-Wave Compression and X-Ray Studies of Titanium Dioxide," *Science*, **155**, 1401-1404 (1967).

[2]See, for example, L. Liu and W.A. Bassett, *Elements, Oxides, Silicates;* pp. 92-195, Oxford Univ. Press/Clarendon Press, New York/Oxford, 1986.

[3]H. Sato, S. Endo, M. Sugiyama, T. Kikegawa, O. Shimomura, and K. Kusaba, "Baddeleyite-Type High-Pressure Phase of TiO_2," *Science*, **251**, 786-788 (1991).

[4]N.A. Bendelianl, S.V. Popova and L.P. Vereschagin, New High Pressure Modification of ZrO_2 and HfO_2", *Geochem. Int.4* 557 (1967).

[5]L.G. Liu, "New High Pressure Phase of ZrO_2 and HfO_2," *J. Phys. Chem. Solids*, **41**, 331 (1980).

[6]D.L. Decker, "High-Pressure Equation of State for NaCl, KCl, and CsCl," *J. Appl. Phys.*, **42** [8] 3239-3244 (1971).

[7]J.C. Jamieson, J.N. Fritz, and M.H. Manghnani, "Pressure Measurement at High Temperature in X-Ray Diffraction Studies: Gold as a Primary Standard"; pp. 27-48 in *High-Pressure Research in Geophysics.* Edited by S. Akimoto and M.H. Manghnani. Center for Academic Publications Japan/Reidel, Tokyo/Dordrecht, 1982.

[8]F. Dachille and R. Roy, "A new high-pressure form of titanium dioxide." *Amer. Ceram. Soc. Bull.* **41**, 225 (1962).

[9]N.A. Bendeliani, S.V. Popova and L.F. Vereschagin, "New Modification of Titanium Dioxide Obtained at High Pressure." *Geokhimiya* **5**, 499-501 (Eng.:Geochem. Int'l. **3**, 387-389) (1966)

[10]J.C. Jamieson and B. Olinger, "High-Pressure Polymorphism of Titanium Dioxide," *Science*, **161**, 893-895 (1968).

[11]J.F. Mammone, S.K. Sharma, and M. Nicol, "Raman Study of Rutile (TiO_2) at High Pressure," *Solid State Commun.*, **34**, 799-802 (1980).

[12]L.C. Ming and M.H. Manghnani, "High-Pressure Phase Transformations in Rutile-Structured Dioxides"; pp. 329-347 in *High-Pressure Research in Geophysics*. Edited by S. Akimoto and M.H. Manghnani. Center for Academic Publications Japan/Reidel, Tokyo/ Dordrecht, 1982.

[13]M. Akaogi, J. Susaki, T. Yagi, K. Kusaba, T. Ato, M. Matsui, and T. Kikegawa, "Accurate Determination of the Phase Boundary of Rutile-α-PbO_2 Transition in TiO_2 Using Synchrotron Radiation"; pp.447-455 in *High-Pressure Research: Application to Earth and Planetary Sciences*. Edited by Y. Syono and M.H. Manghnani. TERRAPUB/American Geophysical Union, Tokyo/Washington, 1992.

[14]T. Mashimo and A. Sawaoka, "Anisotropic Behavior of the Shock-induced Phase Transition of Rutile Phase Titanium-dioxide", *Phys. Lett.*, **78A**, 419-422 (1980).

[15]Y. Syono, K, Kusaba, M, Kikuchi, K, Fukuoka and T. Goto, "Shock-induced Phased Transitions in Rutile Single Crystal."

pp. 385-392 in *High-Pressure Research in mineral physics,* Edited by Y. Syono and M.H. Manghnani. Terra/AGU, Tokyo/Washington, 1987.

[16]K. Kusaba, M. Kikuchi, K. Fukuoka and Y. Syono, "Anisotropic Phase Transition of Rutile under Shock Compression", *Phys Chem Minerals*, **15**, 238-245 (1988).

[17]L. Liu, "A Fluorite Isotype of SnO_2 and a New Modification of TiO_2: Implications for the Earth's Lower Mantle", *Science*, **199**, 422-425 (1978).

[18]J.F. Mammone, M. Nikol and S.K. Sharma, "Raman Spectra of TiO_2-II, TiO_2-III, SnO_2, and GeO_2 at High Pressure", *J. Phys. Chem. Solids*, **42**, 379 (1981).

[19]S. Endo, H. Sato, J. Tang, Y. Nakamoto, T. Kikegawa, O. Shimomura, and K. Kusaba, "Baddeleyite-Type High-Pressure Phase of TiO_2 and Its Stable P-T Region," pp.457-461 in *High-Pressure Research: Application to Earth and Planetary Sciences*. Edited by Y. Syono and M.H. Manghnani. TERRAPUB/American Geophysical Union, Tokyo/Washington, 1992.

[20]H. Arashi, "Raman Spectroscopic Study of the Pressure-Induced Phase Transition in TiO_2," *J. Phys. and Chem. Solids*, **53** [3] 355-359 (1992).

[21]H. Sato, "*In-situ* X-ray Diffraction Study of TiO_2 at High Pressure and High temperature", Master Thesis, Osaka Univ., Toyonaka, Japan, 1991. (in Japanese).

[22]B.G.Hyde, L.A. Bursill, M. O'Keeffe and S. Andersson, "Continuous Topological Variation of Coordination in Crystal: Structural Relations and Possible Transformation Mechanisms," *Nature Phy. Sci.*, **237** 35-38 (1972)

[23]M. O'Keeffe, "On Ten- and Eleven-coordinated Periodic Packings of Equivalent Spheres," *Mat. Res. Bull.*, **19**, 1433-36 (1984)

[24]Y. Kudoh, H. Takeda, and H. Arashi, "*In Situ* Determination of Crystal Structure for High Pressure Phase of ZrO_2 Using a Diamond Anvil and Single Crystal X-ray Diffraction Method," *Phys. Chem. Minerals*, **13**, 233 (1986).

[25]R. Suyama, H. Horiuchi, and S. Kume, "Structural Refinements of ZrO_2 and HfO_2 Treated at 600°C and 6 GPa", *J. Ceram. Soc. Japan*, **95**, 567 (1987).

[26]O. Ohtaka, T. Yamanaka, S. Kume, N. Hara, H. Asano and F. Izumi, "Structural Analysis of Orthorhombic ZrO_2 by High Resolution Neutron Powder Diffraction", Proc. Japan Acad. 66, Ser.B 193 (1990).

[27]O. Ohtaka, T. Yamanaka, S. Kume, E. Ito, and A. Navrotsky, "Stability of Monoclinic and Orthorhombic Zirconia: Studies by High-pressure Phase Equilibria and Calorimetry", *J. Ceram. Soc. Japan*, **74**, 505-509 (1991).

[28]H. Arashi, T. Yagi, S. Akimoto, and Y. Kudoh, "New High-pressure Phase of ZrO_2 above 35 GPa," *Phy. Rev. B*, **41**, 4309 (1990).

[29]G. Bocquillon, C. Susse, and B. Vodar, "High-Pressure Allo-

tropy of Hafnium Oxide"(in Fr.), *Rev. Int. Hautes Temp. Refract.* **5**, 247 (1968).

[30]O. Ohtaka, T. Yamanaka, S. Kume, E. Ito, and A. Navrotsky "Synthesis and X-ray Structural Analysis by the Rietveld Method of Orthorhombic Hafnia", *J. Ceram. Soc. Japan*, **99**, 826 (1991).

[31]D.M. Adams, S. Leonard, D.R. Russell, and R.J. Cernik, "X-ray Diffraction Study of Hafnia under High Pressure Using Synchrotron Radiation," *J. Phys. Chem. Solids*, **52**, 1181-1186 (1991).

[32]Adam and Rogers, *Acta Cryst.*, **12**, 951 (1959).

[33]S. Block, J.A.H. DaJornada, and G.J. Piermarini, "Pressure-Temperature Phase Diagram of Zirconia," *J. Amer. Ceram. Soc.* **68**, 497 (1985).

Acknowledgments

The author would like to express her sincere gratitude to Professor S. Endo for introducing her to this field of research, continual encouragement, stimulating discussions and a critical reading of the manuscript.

She would also like to thank Professors T. Yamanaka, A. Onodera, F. Ono, Drs. K. Suito, M. Togaya, O. Ohtaka, T. Kakeshita, for their stimulating discussions and encouragement.

She wishes to express her thanks to Professor Emeritus F. E. Fujita and S. Kume for their continuing interest and encouragement.

Finally she wishes to thank to Mrs. Y. Kobayashi, and all of the students of Professor S. Endo for their helps in the experiment.